Applied Catalysis B: Environmental 312 (2022) 121436

Contents lists available at ScienceDirect

Applied Catalysis B: Environmental

journal homepage: www.elsevier.com/locate/apcatb

Environmentally benign methane-regulated catalytic desulfurization

Hao Xu [a], Peng He [b], Zhaofei Li [a], Shijun Meng [a], Yimeng Li [a], Lo-Yueh Chang [c], Lijia Liu [d], Xiaodong Wen [b], Brittney A. Klein [e], Vladimir K. Michaelis [e], Jizhen Qi [f], Dongchang Wu [g], Xi Liu [h,*], Hua Song [a,*]

[a] Department of Chemical and Petroleum Engineering, University of Calgary, 2500 University Drive, NW, Calgary, Alberta T2N 1N4, Canada
[b] SynCat@Beijing, Synfuels China Technology Co. Ltd., 1 Leyuan South Street II, Huairou District, Beijing 101407, China
[c] National Synchrotron Radiation Research Center, 101 Hsin-Ann Road, Hsinchu 30076, Taiwan
[d] Department of Chemistry, Western University, 1151 Richmond Street, London, Ontario N6A 5B7, Canada
[e] Department of Chemistry, University of Alberta, 11227 Saskatchewan Drive, Edmonton, Alberta T6G 2G2, Canada
[f] i-Lab, CAS Center for Excellence in Nanoscience, Suzhou Institute of Nano-Tech and Nano-Bionics (SINANO), Chinese Academy of Sciences, Suzhou 215123, China
[g] Shanghai Nanoport, Thermo Fisher Scientific Building A, 2517 Jinke Road, Pudong District, Shanghai 201203, China
[h] In-situ Center for Physical Sciences, School of Chemistry and Chemical Engineering, Shanghai Jiao Tong University, Shanghai 200240, China

ARTICLE INFO

Keywords:
Desulfurization
Methane
Supported catalysts
Green chemistry
Carbon disulfide

ABSTRACT

Hydrodesulfurization is well established in the industry while costly and environmentally unfriendly due to CO_2 emissions and H_2S production. An alternative, cost-effective desulfurization process remains unreported. Here, we demonstrate a desulfurization process for dibenzothiophene, one of the most well-known and recalcitrant sulfur-containing model compounds against catalytic desulfurization, under the regulation of methane instead of hydrogen over a combination of two catalysts, generating a new sulfur-containing product, CS_2, as an important intermediate in organic chemistry and non-polar solvent with lower environmental impact than H_2S. A catalytic mechanism is proposed and supported by extensive experimental and computational evidence. It is discovered that methane acts as a critical initiator and intensifies the direct desulfurization pathway, where two catalysts must work cooperatively and a surface sulfur transfer process is indispensable. This study explores an alternative desulfurization route with unique reaction pathways towards CS_2 formation, whose practical potential is also supported by the desulfurization performance over a series of real-world crude samples.

1. Introduction

Sulfur is the most abundant heteroatom in crude oil, with content ranging from 0.5 to 6 wt%, leading to a series of problems such as sulfur oxide (SO_x) emission and acid rain [1–3]. With the increasing awareness of environmental protection, a desulfurization process to remove sulfur heteroatoms for downstream clean energy utilization has been mandated by multiple pieces of legislation [4]. For example, a maximum sulfur content tolerance of 15 ppm was implemented for on-road vehicles, nonroad vehicles and locomotives in North America in 2006, 2010 and 2012, respectively, with stricter limitations of 10 ppm being introduced in 2017 for gasoline [5]. Starting in 2020, a new regulation implemented by the International Maritime Organization further lowered the acceptable sulfur content in marine oil used by ships outside designated emission control areas from 3.5 to 0.5 wt%. The conventional desulfurization process generally uses H_2 for effective sulfur removal and is thus called hydrodesulfurization (HDS). During this process, H_2 acts as the reductant, and H_2S is formed as the product [6,7]. H_2 is generally produced via methane reforming processes, which are energy-intensive due to the harsh reaction conditions (950–1100 °C, 10 MPa) and the accompanying CO_2 byproduct leads to greenhouse gas emissions [7,8]. In addition, H_2S is notorious for its high toxicity and environmental unfriendliness [9,10]. This combination makes the HDS route both environmentally and economically unfavorable. Alternatively, methane is widely present as the main constituent in natural resources such as natural gas [11]. In recent years, the production of natural gas has increased, and a corresponding price decrease has been observed (from 8.85 USD/million British thermal units at Henry Hub in 2008–2.33 in 2020) [12]. If methane utilization for a desulfurization process is developed, the undervalued commodity could be utilized to circumvent the HDS reforming process [13,14], and the generated H_2S could be replaced with other environmentally benign sulfur products. It

* Corresponding authors.
E-mail addresses: liuxi@sjtu.edu.cn (X. Liu), sonh@ucalgary.ca (H. Song).

https://doi.org/10.1016/j.apcatb.2022.121436
Received 26 January 2022; Received in revised form 5 April 2022; Accepted 18 April 2022
Available online 26 April 2022
0926-3373/© 2022 Elsevier B.V. All rights reserved.

is thus clear that a methane-regulated desulfurization (MDS) process could be beneficial for clean oil production.

This work demonstrates that methane-assisted desulfurization is achievable over a rationally designed dual catalyst system consisting of an MDS1 catalyst ($NiMoS/TiO_2$) for direct desulfurization and a MAC1 catalyst (AgGaCe/ZSM-5) for methane activation (Fig. 1(a)). Dibenzothiophene (DBT) has been used as a representative sulfur-containing model compound for the desulfurization study of heavy oil, as it is notably persistent during desulfurization due to its stable fused-ring structure [15] and is one of the most commonly found

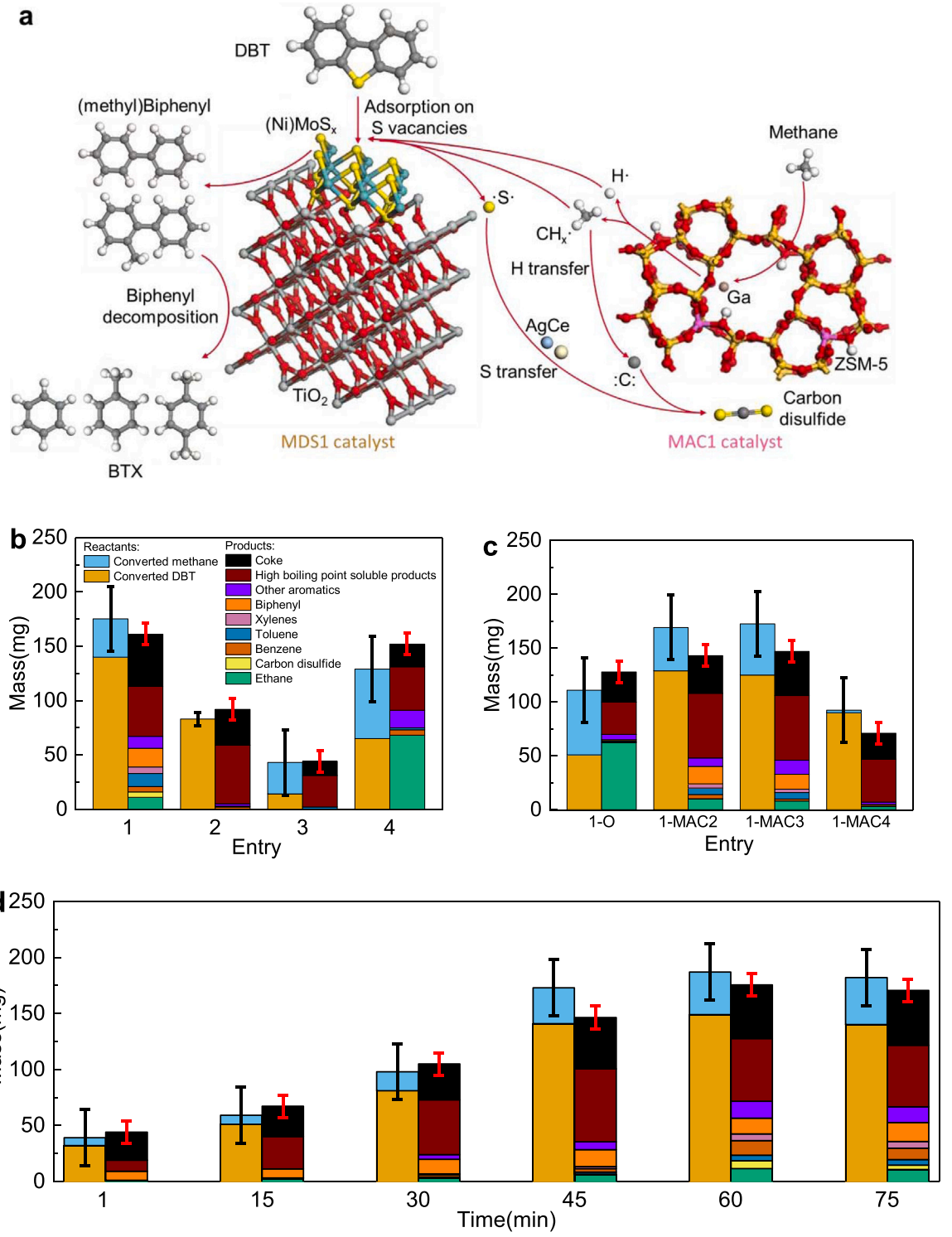

Fig. 1. Mechanism illustration and reaction performances. (a) Proposed mechanism of DBT desulfurization under methane environment. Colors of atoms: yellow for S, teal for Mo, gray for C, white for H, amber for Si, magenta for Al, red for O, coral for Ga and light gray for Ti. (b, c) Quantification of converted reactants and products in entry 1 (main reaction), entry 2 (no CH_4), entry 3 (no MAC1), entry 4 (no MDS1), entry 1-O (MDS1→MDS1-O), entry 1-MAC2 (MAC1→MAC2 (no Ag)), entry 1-MAC3 (MAC1→MAC3 (no Ce)) and entry 1-MAC4 (MAC1→MAC4 (no Ga)). Hydrogen is not illustrated in the columns for products because the mass contribution is negligible. (d) Quantification of converted reactants and products in entry 1 at different reaction times. (b~d) share the same legend and the error bars represent the standard deviation for measurements.

sulfur-containing components in petroleum, especially in heavy oil [16]. Therefore, if DBT desulfurization occurs in a methane environment, it is likely that other sulfur-containing species can also be effectively converted. Upon subjecting DBT to an MDS process, an environmentally benign sulfur-containing product carbon disulfide (CS_2) was formed, which, to the best of our knowledge, has never been publicly reported. Control experiments show that methane, MDS1 and MAC1 are all essential for this desulfurization route. ^{13}C isotope labeling studies suggest the participation of activated methane in the reaction, while ^{34}S isotope experiments indicate that the sulfur atom in DBT is adsorbed and interchanged with sulfur vacancies in MDS1, triggering the subsequent reactions. Catalysts and product characterizations, additional control experiments and theoretical calculations were performed to validate the proposed reaction mechanism. It can be seen that methane-regulated desulfurization is a more complex process than the hydrodesulfurization process. Methane plays an essential role as an initiator to intensify a direct desulfurization pathway, and ends up being incorporated into final products, majorly in ethane and aromatic derivatives, while minorly in carbon disulfide. In addition to the presence of methane, the abundance of sulfur vacancies and the surface sulfur transfer process are also crucial for the successful desulfurization and the formation of carbon disulfide. Therefore, unique catalyst design is paramount in this MDS process. The MDS of several typical real-world samples was also carried out. Favorable desulfurization performance and catalyst stability were observed, further indicating that the process has great potential to provide a more economically feasible and environmentally friendly alternative for the oil processing industry.

2. Experimental

2.1. Catalyst preparation

The dual catalyst system was prepared by the mechanical mixing of two different components, MDS1 and MAC1.

The typical synthesis procedure of MDS1 is as follows. Ammonium tetrathiomolybdate (ATM, $(NH_4)_2MoS_4$) was used as the sulfur precursor in the preparation of the MDS1 catalyst. First, 25.0000 g ammonium heptamolybdate tetrahydrate (AHM, $(NH_4)_6Mo_7O_{24}{\cdot}4H_2O$, 98–102 wt %, VMR) was dissolved in 100 mL ammonia aqueous solution (28–30 wt %, Sigma-Aldrich) in a beaker set on a hot plate at 60 °C. Then, 225 mL $(NH_4)_2S$ solution (20 wt%, Sigma-Aldrich) was added under constant stirring. After 1 h, the solution was put in a refrigerator at 4 °C for 6 h to facilitate the precipitation and crystallization of the resulting ATM. The produced crimson crystal of ATM was further filtered and rinsed by deionized water and ethanol three times respectively and stored in closed vials in the refrigerator to prevent oxidation. To get the MDS1 catalyst, 1.3014 g ATM was firstly dissolved in 25 mL deionized water. Meanwhile, 0.6250 g nickel nitrate hexahydrate ($Ni(NO_3)_2.6\ H_2O$, 98 wt%, Alfa Aesar) was dissolved in 5 mL deionized water. Then, the two solutions were loaded dropwise on 5.0000 g TiO_2 support (P25, >99.5 wt%, Sigma-Aldrich) via stepwise impregnation and the resultant was fully dried at 110 °C overnight in an oven to get a uniform powder with crimson color. Finally, the powder was treated in a tube furnace with an inert He flow (>99.999%, Air Liquide, 100 mL min^{-1}) at 350 °C for 2 h. The produced black powder ($NiMoS/TiO_2$) was collected and denoted as MDS1. The MDS1 catalyst was stored in closed vials under an inert N_2 atmosphere to avoid partial oxidation, which could lead to catalyst deactivation.

MAC1 was prepared through stepwise impregnation according to a similar procedure in our previous publications [17]. First, NH_4-ZSM-5 with a silica to alumina ratio of 23:1 was purchased from Zeolyst, USA. It was further converted into HZSM-5 through calcination at 600 °C in the air atmosphere for 5 h. Next, the metal-loaded HZSM-5 catalyst was prepared by a stepwise impregnation method. In the first step, 0.0744 g $AgNO_3$ (>99.0 wt%, Sigma-Aldrich) and 0.3441 g $Ga(NO_3)_3{\cdot}xH_2O$ (99.9 wt%, Sigma-Aldrich) were dissolved in 7 mL deionized water. The solution was loaded dropwise on 5.0000 g of the aforementioned zeolite support under vigorous stirring. Then, the catalyst was fully dried at 110 °C overnight in an oven and calcined at 550 °C for 4 h afterward and denoted as AgGa/ZSM-5. In the second step, 0.7747 g Ce $(NO_3)_3{\cdot}6H_2O$ (99 wt%, Sigma-Aldrich) was dissolved in deionized water and the solution was loaded dropwise on the prepared AgGa/ZSM-5. Then, the catalyst was fully dried at 110 °C overnight in an oven and calcined at 550 °C for 4 h afterward. The resulting white powder (AgGaCe/HZSM-5) was collected and denoted as MAC1.

2.2. Performance evaluation

The DBT desulfurization reaction under a methane environment was carried out in a batch reactor at 400 °C for 1 h. A typical reaction procedure was as follows. First, 0.4000 g dual catalyst system was prepared by mechanical mixing of 0.2000 g MDS1 and 0.2000 g MAC1 components. Then, the catalyst was added in a 100 mL batch reactor manufactured by Parr Instrument USA, which can be used at high temperature of up to 500 °C and high pressure of up to 5000 psi (34.5 MPa). 1.0000 g DBT (98 wt%, Sigma-Aldrich) was directly used as a solid feedstock without using other solvents for the simplicity of the reaction system, so that the mechanism can be better investigated. The reactor was sealed by flange to a multifunctional reactor top equipped with a stirrer, thermocouple, pressure gauge and circulated cooling water system. Next, a standard gas mixture consisting of 89.8 mol% CH_4 and 10.2 mol % N_2 (Air Liquide) was used to purge the reactor three times through a connected tubing system and then pressurize the reactor to 3.5 MPa. Here, N_2 was introduced as an internal standard to calculate methane conversion after the reaction. The reactor was then put on the scale for a leak test, where the mass and pressure of the reactor were confirmed to be stable. After passing the leak test, the reactor was put into a temperature-controlled heating furnace and heated up to the desired reaction temperature of 400 °C through a PID controlling system. The temperature ramping stage lasted 20 min and then the reactor was maintained at 400 °C for 1 h. After the time was up, the reactor was cooled down to room temperature with the assistance of external air flow.

2.3. Product analyses

After the reaction, the products in the gas, soluble and solid phase were analyzed respectively as follows:

1. Gas phase: the product gas was directly fed into a micro-chromatography (micro-GC) to analyze the gas composition. Instrument and conditions: four-channel micro-GC (490, Agilent) equipped with thermal conductivity detector (TCD). The first channel was equipped with a 10 m molecular sieve 5 A column to analyze H_2, O_2, N_2, CH_4 and CO; the second channel was equipped with a 10 m PPU column to analyze CO_2, C_2H_6 and C_2H_4; the third channel was equipped with 10 m alumina column to analyze $C_4{\sim}C_6$ hydrocarbons; the forth channel was equipped with 8 m CP-Sil 5CB column to analyze C_3H_8 and C_3H_6. Temperature and pressure of columns: 80 °C and 200.0 kPa (first), 100 °C and 175.0 kPa (second), 80 °C and 180.0 kPa (third), 100 °C and 85.0 kPa (fourth), analysis time: 2.5 min. The carrier gas was Ar (99.999%, Air Liquide) and internal standard N_2 (99.999%, Air Liquide) in mixed gas was used to calculate the methane conversion in each reaction. A residual gas analyzer (Cirrus 3) was also used to provide the mass spectra of gas-phase products under certain circumstances.
2. Soluble phase: after reaction, 10.00 g 1,1,2,2-tetrachloroethane (TCE, >99.0%, EMD Millipore Corp.) was injected into the reactor as the solvent to extract all soluble products. Then the soluble and solid products were collected together and then separated through a medium rate filtering paper. The collected soluble products in TCE solvent were sealed in vials and kept in a refrigerator to minimize the

loss of volatile fractions. The DBT concentration in the product solution was measured by a UV-Visible spectrometer. DBT has a characteristic absorbance peak at 325 nm, which complies well with the linear relationship in Beer-Lambert law (Fig. S1) and is free of interference from the solvent and other generated products. For a typical measurement, 0.1 mL product solution was diluted in 3 mL toluene (99.9%, Anachemia) and well mixed. The diluted solution was diluted in the same manner (0.1 mL in 3 mL toluene) another time and placed into a cuvette (4.5 mL, 10 mm) after sufficient mixing. Then the cuvette was set in a UV-Visible spectrometer (Thermo Fischer) to obtain the spectra. Instrumental settings: wavelength range 300–350 nm, scan rate 1 nm s^{-1}, scan interval 0.5 nm. The DBT concentration in the original product was then calculated by the multiplication of deduced DBT concentration in the calibration curve and the dilution factor.

Also, the collected solution was further injected into a gas chromatography-mass spectroscopy (GC-MS) to get the corresponding composition of species with boiling points lower than 250 °C. Instrument and conditions: GC-MS (PerkinElmer GC Claus 680 and MS Clarus SQ 8 T) equipped with a capillary column designed to analyze paraffin-olefin-naphthene-aromatic (PONA) components (Agilent HP-PONA). A stepwise temperature ramping program was set during the analysis and the corresponding curve was shown in Fig. S2. Standard PONA species with 5–11 carbon numbers were used to calibrate the GC-MS by establishing a working curve to correlate the concentration of each species and the peak area in the chromatogram so that the amount of each product in the liquid phase can be determined. During the analysis process, the peaks in the chromatogram were designated by comparing the mass spectra with standard compounds in the purchased National Institute of Standards and Technology (NIST) database and selecting the most probable hit.

In order to get the content of soluble species with boiling points higher than 250 °C (referred to as high boiling point soluble products hereinafter), simulated distillation analysis (SDA) was carried out. Instrument and conditions: Agilent 8890 GC system equipped with a 30 m HP-5 column and an FID detector. The results were analyzed by SimDis Expert software from Separation Systems to get the boiling point curves. Liquid nitrogen was used to realize the cryogenic GC analysis from − 20 °C to 450 °C with a temperature ramping rate of 10 °C min^{-1}. A typical boiling point curve for the quantification of high boiling point soluble products is shown in Fig. S3.

3. Solid phase: the solid product was collected and subjected to thermogravimetric analysis (TGA) to determine the amount of coke formation during the process. TGA measurements were performed with a simultaneous thermal analyzer (PerkinElmer STA 6000). The samples were held at 30 °C for 5 min for a stable initial weight, then ramped to 800 °C at a rate of 20 °C min^{-1} under 30 mL min^{-1} air flow and held for 5 min. Typical TGA curves for the MDS1 catalyst before and after the reaction are shown in Fig. S4. The weight loss from 350 °C to 800 °C was attributed to coke oxidation after excluding the contribution from the loss of sulfur in this temperature range.

After getting all relevant data, the corresponding values for product analysis were calculated according to the following equations:

$$\text{Methane conversion} = \left(1 - \frac{\text{mole of remaining methane after reaction}}{\text{mole of fed methane}}\right) \times 100\%$$

$$\text{Soluble yield} = \frac{\text{mass of solubles in product}}{\text{mass of fed DBT}} \times 100\%$$

$$\text{Gas yield} = \frac{\text{mass of produced gas in product}}{\text{mass of fed DBT}} \times 100\%$$

$$\text{DBT conversion} = \left(1 - \frac{\text{mass of remaining DBT after reaction}}{\text{mass of fed DBT}}\right) \times 100\%$$

$$\text{Coke yield} = \frac{\text{mass of coke in product}}{\text{mass of fed DBT}} \times 100\%$$

For a specific product species A, the yield was also based on the mass of solid DBT feedstock as shown in the following equation:

$$\text{Yield of A} = \frac{\text{mass of produced A in product}}{\text{mass of fed DBT}} \times 100\%$$

2.4. Control experiments

In order to further validate the function of methane and two components in the dual catalyst system during the DBT desulfurization process, a series of control experiments were also designed and performed. The main reaction was named entry 1 (CH_4 +MDS1 +MAC1). This reaction was repeated three times to evaluate the uncertainties of the measurements and obtain confidence intervals for the collected data. Entry 2 (N_2 +MDS1 +MAC1) followed similar conditions in entry 1 and the only difference was that pure nitrogen was introduced instead of methane to the same pressure of 3.5 MPa. Entry 3 (CH_4 +MDS1) followed similar conditions in entry 1, whereas the MAC1 component was not added in the catalyst. Entry 4 (CH_4 +MAC1) followed similar conditions in entry 1, whereas the MDS1 component was not added. Besides, Entry 0 (CH_4 +SiC) was also designed as a background reaction using unreactive solid SiC to explore possible thermal reactions between DBT and methane under given reaction conditions.

MDS1-O ($NiMoO/TiO_2$) catalyst was prepared to test whether the sulfide-form MDS1 catalyst can be replaced by an oxide-form counterpart for the MDS process. This oxide-form MDS1-O catalyst was prepared using the same types and amounts of metal precursors ($(NH_4)_6Mo_7O_{24}{\cdot}4H_2O$ and $Ni(NO_3)_2{\cdot}6H_2O$) and support (TiO_2) used for the preparation of MDS1. The only difference is that sulfur precursor ($(NH_4)_2S$) was not added during the preparation process. Entry 1-O (CH_4 +MDS1-O+MAC1) followed similar conditions in entry 1, but the MDS1 component in the catalyst was replaced by MDS1-O.

MAC2 (GaCe/ZSM-5, no Ag), MAC3(AgGa/ZSM-5, no Ce) and MAC4 (AgCe/ZSM-5, no Ga) catalysts were also synthesized to investigate the function of three metal components in MAC1 (AgGaCe/ZSM-5) catalyst. The experiments using MAC2, MAC3 and MAC4 to replace MAC1 in entry 1 were labeled as entries 1-MAC2, 1-MAC3 and 1-MAC4, respectively. Other reaction conditions were kept the same as entry 1 in these experiments.

The experiments with controlled reaction time were also carried out and labeled as entry 1-X min, where X (with the values of 1, 15, 30, 45, 60, 75, respectively) represents the reaction time in minutes. This series of experiments followed similar conditions in entry 1, while the reactor was quenched in cool water at the set reaction time.

The main reaction and control experiments are further summarized

in Table S1.

2.5. Isotope labeling experiments

In order to track the participation and evolution of methane in the MDS process, a ^{13}C isotope labeling experiment was carried out. This reaction was denoted as entry 1–13 C, which adopted a similar reaction process in entry 1, and the only difference was the use of ^{13}C concentrated CH_4 as the feed gas. After the reaction, the separated soluble phase and solid phase were sealed for further analyses, respectively. For the soluble phase, 0.1 g sample was first diluted in 1 g deuterochloroform ($CDCl_3$). Then, ^{13}C nuclear magnetic resonance (NMR) was conducted at 9.4 T ($\nu_L(^{13}C) = 100.6$ MHz) on a Bruker Avance III 400 spectrometer with a BBFO 5 mm probe. The chemical shifts were referenced to $CDCl_3$ at 77.26 ppm. A spectral width of 24 kHz was used to acquire 1024 scans per spectrum. For solid samples, solid-state nuclear magnetic resonance (SS NMR) measurements were acquired on a 9.39 T Bruker Avance III HD spectrometer ($n_L(^1H) = 400.1$ MHz, $n_L(^{13}C) = 100.6$ MHz) equipped with a 4 mm double resonance (H-X) Bruker magic-angle spinning (MAS) NMR probe. $^{13}C\{^1H\}$ cross-polarization (CP) MAS NMR experiments were performed using a 4.1 μs 90° pulse on ^1H and a ramped Hartman-Hahn match on ^{13}C [18]. An optimized contact time of 2–3 ms ($\gamma B_1/2\pi$ of 61 kHz on ^1H) was employed for all ^{13}C CP experiments collecting 2048 co-added transients with recycling delays of 10 s. Each experiment was performed at ambient temperature using a MAS frequency of 13 kHz. All ^{13}C spectra were referenced to the high-frequency peak of adamantane ($\delta = 38.56$ ppm) and utilized TPPM ^1H decoupling ($\gamma B_1/2\pi = 61$ kHz) [19]. All data were processed in TOPSPIN using 50–100 Hz line broadening.

Besides, two MDS catalysts made from natural elemental sulfur and ^{34}S concentrated elemental sulfur were prepared as follows. First, 0.1840 g ammonium heptamolybdate tetrahydrate (AHM, $(NH_4)_6Mo_7O_{24}{\cdot}4H_2O$, 98–102 wt%, VMR) and 0.0619 g nickel nitrate hexahydrate ($Ni(NO_3)_2{\cdot}6H_2O$, 98 wt%, Alfa Aesar) were dissolved in 1 mL deionized water at room temperature. Then, the solution was loaded dropwise on 1.0000 g TiO_2 support (P25, >99.5 wt%, Sigma-Aldrich) and dried at 110 °C overnight. Next, the product was put into a tube furnace, heated up to 600 °C and held for 4 h with the temperature ramping rate of 10 °C min^{-1} under 100 mL min^{-1} Ar flow. The obtained material was ground together with 0.2000 g elemental sulfur in a mortar and dispersed in ethanol. Ultrasonic treatment was applied for better mixing of the two components and ethanol was subsequently evaporated in an oven set at 80 °C overnight. Finally, the powder was calcined in a tube furnace under 100 mL min^{-1} inert Ar flow at 600 °C for 24 h with the temperature ramping rate of 1 °C min^{-1}. The produced black powder was collected and denoted as MDS-S. A similar procedure was performed while the natural elemental sulfur was replaced by ^{34}S concentrated elemental sulfur, and the corresponding catalyst was denoted as MDS-34S. These two catalysts were used for MDS reactions and the experiments were labeled as entry1-S and entry1–34S correspondingly.

2.6. Catalyst characterization

X-ray adsorption fine structure (XAFS) of the samples was examined at National Synchrotron Radiation Research Center (NSRRC), Hsinchu, Taiwan. The XAFS at the Mo and Ni K-edge were measured at BL44A (Taiwan Photon Source), and the S K-edge XAFS were measured at the BL16A (Taiwan Light Source). All spectra were collected in fluorescence mode. Standards such as Mo, MoO_3, MoS_2, Ni, NiO and Ni_3S_2 were measured in the transmission mode. The EXAFS data were processed using ATHENA [20]. The fitting was performed using the IFEFFIT package with FEFF6L [21]. All spectra were fitted to a straight line for the pre-edge region and a cubic spline for the post-edge background. Then the post-edge background was subtracted from the spectra and normalized with respect to the edge jump step to get the EXAFS function. Besides MDS1 and MDS1-O, the used MDS1 sample after the desulfurization process was also characterized and labeled as MDS1-Used.

X-ray diffraction (XRD) was used to confirm the possible crystalline structure in fresh/spent catalysts. Instrument and conditions: D2 Phaser diffractometer with Cu K_α irradiation (Bruker, Germany), working voltage: 20 kV, working current: 40 mA. Scanning range: 2θ= 3°-90°, scanning speed: 3° min^{-1}.

X-ray photoelectron spectroscopy (XPS) was used to determine the valence and chemical environment of important elements in fresh/spent catalysts. Instrument and conditions: Thermo Scientific ESCA-LAB 250Xi X-ray photoelectron spectrometer equipped with a hemispherical electron energy analyzer (Bruker, Germany). X-ray source: Al K_α ($h\nu = 1486.6$ eV) with a spot size of 650 μm. The electron energy analyzer was operated at constant pass energy of 20 eV to acquire detailed scans.

Scanning/transmission electron microscopy (STEM) was used to observe the microscopic structure and the distribution of important elements in fresh/spent catalysts. Instrument and conditions: ThermoFisher ThemisZ probe-corrected scanning/transmission electron microscope equipped with SuperEDX, a Gatan GIF Quantum 965 energy filter and a segmented 4-quadrant STEM DF4 detector, which was operated at 300 keV. The catalyst samples were directly dry dispersed on Cu grids without further treatments like plasma cleaning before the STEM characterizations. In order to image beam-sensitive molecular sieve samples and adsorbents in channels, the samples were characterized under a low-dose mode (<0.1 pA) using the segmented DF4 detector [22]. The rest of the STEM images were recorded with a dose rate of about 50 pA if experimental conditions were not mentioned additionally. In order to attain secondary electron images of catalysts with atomic resolutions, Hitachi HF-5000 probe-corrected STEM equipped with a secondary electron detector was employed, which was operated at 200 keV.

2.7. Mechanism study

In order to substantiate the mechanism of DBT desulfurization and the evolution of other products, a series of verification experiments were designed and performed as follows.

In the main reaction (entry 1), two catalyst components MDS1 and MAC1 were mechanically mixed before the reaction. In order to further differentiate the function of each component, two new experiments in which two catalyst components were separated by vial were carried out. In one experiment denoted as MDS1 +DBT|MAC1, MAC1 was firstly put in the reactor while MDS1 and DBT were put in a 10 mL glass vial with an open mouth and then set in the reactor. After the reaction, the soluble and solid products inside the vial and outside the vial were collected and analyzed separately. In another experiment denoted as MAC1 +DBT|MDS1, MDS1 was put in the reactor outside the vial while MAC1 and DBT were added inside the vial. The reaction and sample analyses were performed in a similar manner.

Two background reactions using the mixed gas (89.8 mol% CH_4 and 10.2 mol% N_2) as the only feedstock were also performed to evaluate the capability of two catalyst components for methane activation, which is the essential first step to trigger the MDS process. The two reactions with MDS1 and MAC1 catalyst were labeled as M1 and M2, respectively.

Biphenyl is observed as an important product in the MDS process, and the subsequent decomposition of biphenyl produces valuable products including benzene, toluene and xylenes. Therefore, the decomposition of biphenyl was also studied by using biphenyl as the solid feedstock. The reactions with the sole presence of MDS1 and MAC1 catalyst were denoted as entry Bph1 and Bph2, respectively.

In order to further confirm the possibility of methane incorporation through alkylation of the aromatic ring, experiments using benzene as the feedstock were carried out. The reaction using MDS1 catalyst was labeled as B1, and the one using MAC1 was labeled as B2, correspondingly.

Carbon disulfide is another important product detected in the MDS process, which is never reported in the HDS process to the best of our knowledge. In order to check whether CS_2 is stable as a final product in the MDS process, a control experiment using CS_2 as the feedstock was performed and labeled as entry CS2.

In order to investigate the influence of side-chain substituents connected to the DBT molecule on its convertibility, control experiments with 4-methylDBT and 4,6-dimethylDBT as the solid feedstock were performed. These experiments also aid to check the possible steric effects from the alkyl group(s) close to the sulfur atom in the DBT structure, which is also informative for the mechanistic understanding of the DBT desulfurization process. These entries were labeled as 4MDBT and 46DMDBT, respectively.

More evidence of the CS_2 formation process was acquired through the reaction of methane and/or biphenyl over a sulfurized MAC1-S catalyst, which was prepared by treating MAC1 under 100 mL min^{-1} 1 mol% H_2S (Ar balance) for 4 h. The reactions using MAC1-S as the catalyst and methane + biphenyl, methane, biphenyl (N_2 atmosphere) and methane + benzene as the reactant(s) were labeled as MAC1-S1, MAC1-S2, MAC1-S3 and MAC1-S4, respectively. Besides, an isotope labeling experiment using biphenyl and $^{13}CH_4$ as the feedstock was also performed and denoted as MAC1-S1–13 C.

A silica-coated MAC1 catalyst was prepared to confirm the indispensable role of surface carbonaceous species over the MAC1 catalyst for the formation of CS_2. The catalyst MAC1 @Si was prepared according to the following steps. First, 0.3441 g $Ga(NO_3)_3{\cdot}xH_2O$ (99.9 wt%, Sigma-Aldrich) was dissolved in 7 mL deionized water, and the solution was loaded dropwise onto 5.0000 g HZSM-5 zeolite, which was the same support used for the preparation of MAC1, under vigorous stirring. Then, the catalyst was fully dried at 110 °C overnight in an oven and calcined at 550 °C for 4 h afterward and denoted as Ga/ZSM-5. Next, 1.0000 g prepared Ga/ZSM-5 was put in 40 mL anhydrous ethanol and 2.50 g 3-aminopropyltriethoxysilane (APTEOS, Sigma-Aldrich) was added dropwise under vigorous stirring. The mixture was dried at 70 °C until ethanol was fully vaporized, and calcined again at 550 °C for 4 h. The resultant catalyst was labeled as Ga/ZSM-5 @Si. Finally, 0.0149 g $AgNO_3$ (>99.0 wt%, Sigma-Aldrich) and 0.1549 g $Ce(NO_3)_3.6\ H_2O$ (99 wt%, Sigma-Aldrich) were dissolved in 1.4 mL deionized water and the solution was loaded dropwise onto the Ga/ZSM-5 @Si. The catalyst was fully dried at 110 °C overnight in an oven and calcined at 550 °C for 4 h afterward. The resulting white powder was collected and denoted as MAC1 @Si. The reaction using MDS1 and MAC1 @Si as the catalysts was further carried out and labeled as entry MAC1 @Si.

The abovementioned confirmation experiments are summarized and listed in Table S2.

2.8. DFT calculations

Vienna ab initio simulation package (VASP) was used in this study for density functional theory (DFT) calculations [23]. First-principles calculations with the projector-augmented wave (PAW) method were adopted [24]. The generalized gradient approximation (GGA) functional of Perdew, Burke and Ernzerhof (PBE) was selected as the exchange and correlation potentials [25]. Gaussian smearing with a width of 0.01 eV was used and the method of conjugate gradient energy minimization was chosen for geometry relaxation. The total energy was converged to lower than 10 meV with a plane wave cutoff of 400 eV and a $3 \times 3 \times 1$ Monkhorst–Pack k-point sampling was adopted for the Brillouin zone. In order to study the adsorption of DBT, 4-methylDBT and 4,6-dimethylDBT on MoS_2, a $3 \times 3 \times 1$ supercell of MoS_2 containing 75 atoms was constructed with a removed center S atom to mimic the sulfur vacancy. A vacuum space of 20 Å was applied to avoid the multilayer interaction of the periodic structure. As the input of geometry optimization, methane and the sulfur species (DBT, 4-methylDBT and 4,6-dimethylDBT) were placed on the top site of the sulfur vacancy. Besides, an MFI zeolite structure from International Zeolite Association was used, which contained 96 Si atoms and 192 O atoms to simulate the ZSM-5 structure [26,27]. In order to meet the silica to alumina ratio of 23:1, 8 Si atoms were replaced by Al. Then, the adsorption of methane and DBT on the MAC1 catalyst structure was calculated using a zeolite cell with the gamma point. Acceptable convergence was obtained within 100 steps for all calculations.

2.9. Real-world sample evaluations

Four typical real-world oil samples were selected to evaluate the practical desulfurization performance of the MDS process. 1) Marine diesel oil is a kind of fuel oil widely used by medium and high-speed ships in the maritime field due to its cost advantage. 2) Renewable diesel oil is a type of fuel with similar chemical compositions as petroleum diesel, which is derived from waste agricultural products such as vegetable oils, fats, and greases. 3) Coker naphtha is a naphtha distillate derived from the coker unit through a thermal cracking process. It generally contains a much higher amount of sulfur and olefins than straight-run naphtha, challenging the downstream hydrotreating process. 4) Heavy crude oil is a type of natural petroleum sample with a density of 0.9637 g mL^{-1} and a viscosity of 2262 mPa·s.

First, a batch reactor was used to provide an initial assessment of the desulfurization performance for four oil samples. The instruments and conditions were similar to those used for model compound DBT as described in Section 2.2. The only difference was that the amount of catalyst (0.4000 g MDS1 and 0.4000 g MAC1) and oil feedstock (2.00 g) were doubled simultaneously so that sufficient product oil could be collected for measurement purposes. Good miscibility of methane in all oil feedstocks can be achieved in these experiments. To verify the formation of CS_2, the liquid product collected from the heavy crude oil desulfurization process was left in the reactor after the degassing process and heated up to 70 °C for the detection of volatile components. Nitrogen gas was used as the carrier gas and the sample was introduced to a residual gas analyzer (Cirrus 3, MKS Instruments) to get the mass spectra. It should be pointed out that adsorptive desulfurization also contributes to the final desulfurization performance, while a previous work confirms that catalytic desulfurization under a methane environment also plays an important role for real-world samples [28].

Furthermore, a 7-day long-term stability test was also carried out in Microactivity Effi fixed bed reactor (Micromeritics) using coker naphtha as the oil feedstock. In this reaction, an equivalent amount of MDS1 and MAC1 catalysts were mechanically mixed in an agate mortar and shaped into cylinders with 0.5 cm diameter and 0.5 cm length by a pellet press with a pressure of 20 MPa for 3 min. Then, the catalyst pellets were loaded into the tubular reactor with a thermal couple directly placed in the catalyst bed for temperature measurement. Next, the reactor was sealed and a leaking test was carried out by feeding nitrogen gas to confirm that the pressure could be maintained. Subsequently, the reactor system was heated up to 400 °C and pressurized to 3 MPa in a hot box whose temperature was maintained at 180 °C. Finally, after the stable conditions were reached, the oil was introduced through a high-pressure pump to start the reaction. The LHSV (liquid hourly space velocity) was kept at 2 h^{-1} and the gas (90% CH_4, 10% N_2) to liquid ratio was maintained at 1500:1 during the reaction. A high-pressure liquid/gas separator was used to separate liquid and gas products after the reactor, and the oil products were collected no longer than every 12 h.

The sulfur content in all feedstock and product oils was measured by inductively coupled plasma-optical emission spectrometry (ICP-OES) on an iCAP 7000 SERIES ICP spectrometer (Thermo Scientific). The sample was first dispersed in PermiSolv™, which is a standard solvent for oil analysis. Then, the solution was measured at least three times to get the standard deviation and the sulfur content in each sample was calculated by multiplying the dilution factor.

3. Results and discussion

3.1. Initial catalyst design and reaction evaluation results

3.1.1. Selection of MDS1 catalyst

Since DBT is one of the most stable sulfur-containing compounds in the heavy fraction of crude oil, the corresponding desulfurization process cannot proceed without a rational catalyst design. First, a catalyst with strong sulfur adsorption capability must be present to effectively capture the sulfur atom in DBT, so that the separation of the S atom from the cyclic structure of DBT could occur through C-S bond scission [29]. This process is similar to the direct desulfurization (DDS) pathway in the HDS process. Therefore, a catalyst with high DDS activity in HDS could also be a good starting point for the MDS process. It is widely reported that molybdenum sulfide catalysts supported by metal oxide and promoted by nickel/cobalt demonstrates satisfactory DDS activity [30]. Therefore, an optimized NiMoS/TiO_2 catalyst from previous studies was adopted as an initial attempt [30]. This catalyst component is denoted as MDS1 for its function as a desulfurization catalyst under a methane environment.

3.1.2. Selection of MAC1 catalyst

In a typical HDS process, after C-S bond scission via the DDS pathway, H atoms need to be added to the aromatic ring of the sulfur-free part to form a stable biphenyl structure. The necessity of extra H atoms can be clearly seen from the formula of reactant DBT ($C_{12}H_8S$) and product biphenyl ($C_{12}H_{10}$): two hydrogen atoms are needed for converting one DBT molecule. Therefore, the presence of active H atoms could greatly facilitate the desulfurization process. Similarly, if the MDS process can be realized, a corresponding radical generated from methane (including hydrogen and methyl radicals) should also be added to the aromatic ring structure to form a stabilized final product, and the activation of methane is thus essential for triggering subsequent reactions. The catalyst for methane activation was extensively studied in our previous work [17,31–34]. A specific catalyst with optimized methane activation ability was selected and employed, which is denoted as MAC1 for its function as a methane activation catalyst.

3.1.3. Reaction performance of dual catalyst system for DBT desulfurization

DBT desulfurization in a methane environment was carried out over a dual catalyst system (entry 1). It should be noted that although both MDS1 and MAC1 are prepared with reference to previous work, the creative combination of these two catalysts has never been reported, to the best of our knowledge. The overall analysis results with estimated error ranges are shown in Table S3, proving the rationality and reliability of the adopted methods for high-quality quantitative measurements. Acceptable mass, carbon and sulfur balances based on converted reactants are also verified in Table S4. The slightly low sulfur balance could be due to the loss of volatile sulfur-containing products such as carbon disulfide (boiling point 46 °C) during the measurement process. The detailed distribution of converted reactants and formed products are shown in Fig. 1(b). Entry 1 shows 1.4% methane conversion and 14.0% DBT conversion, which cannot be fully attributed to experimental error, indicating the occurrence of reactions. Although the 1.4% methane conversion is limited, if the absolute mass of converted methane (35 mg) and DBT (140 mg) are compared (Fig. 1(b) and Table S4), the contribution of methane is not negligible. In the gas phase, ethane is observed as the main product, and trace amounts of H_2 are detected. However, H_2S is not detected in the gas phase, which is a stark difference from the results of the traditional HDS process. In the soluble phase, CS_2 is clearly observed as a product, which is distinctive to the MDS process. Compared with H_2S, CS_2 has much lower toxicity. It is widely used as a solvent for both organic and inorganic non-polar substances, as well as intermediate for synthetic fibers, films and organosulfur compounds [35,36]. Therefore, the production of CS_2, although the amount is temporarily limited, deserves extra attention. Furthermore, considerable quantities of other valuable products such as benzene, toluene and xylenes (BTX), are also detected. These products might originate from the decomposition of biphenyl, which has also been observed and widely reported in the direct desulfurization (DDS) pathway in the HDS process, indicating the occurrence of DDS reactions in the MDS process [37]. However, typical products generated from the hydrogenation (HYD) pathway in the HDS process such as cyclohexylbenzene are not observed, confirming the absence of HYD reactions in the MDS process [37]. The dominance of DDS over the HYD mechanism in the methane-regulated DBT desulfurization process circumvents the unnecessary saturation of aromatics in the conventional HDS process, favoring a higher molecular efficiency for desulfurization. In addition, the presence of high-boiling-point soluble products, as confirmed by simulated distillation (Fig. S3), and coke, as confirmed by thermal gravimetric analysis (Fig. S4), suggests the occurrence of polymerization and coking reactions.

3.2. Control experiments

3.2.1. Indispensable role of CH_4, MDS1 and MAC1

Control experiments (entries 2–4) were further performed and the overall analysis results are shown in Table S5. The distribution of converted reactants and formed products is further compared with that of entry 1 in Fig. 1(b). By comparing entries 1 and 2 (no CH_4), it is evident that a larger range of soluble products is generated in the presence of methane but not under a nitrogen environment, supporting the important role of methane in the reaction for the formation of valuable products. Notably, the facilitation of DBT desulfurization after methane introduction leads to the co-utilization of methane and sulfur-containing compounds, converting intractable and low-value-added reactants into valuable products, which is highly meaningful from both economic and environmental standpoints. By comparing entries 1 and 3 (no MAC1), it can be seen that methane conversion decreases dramatically in the absence of MAC1, suggesting the essential role of MAC1 in methane activation. Considering the inert nature of methane due to its stable structure and high C-H bond energy of 435 kJ mol^{-1} (the highest among hydrocarbons), this conclusion is undoubtedly reasonable: unlike the HDS process, which involves the intrinsic high activity of H_2, the MDS process is triggered by a rationally designed catalyst for methane activation [38,39]. This conclusion also explains the lack of reports on the MDS process to date, since the feasibility is extremely low if only a conventional HDS catalyst, which is not capable of methane activation, is employed. As seen by comparing entries 1 and 4, although methane conversion can be even higher over MAC1 in the absence of MDS1, the activated methane molecules are almost fully converted to ethane since the mass of converted methane is similar to that of produced ethane. The predominant formation of ethane can be explained by the self-combination of methyl radicals after methane activation, which was commonly reported in our previous studies [40,41]. As determined from entry 1, the presence of MDS1 enables a new desulfurization pathway, which competes with the formation of ethane. Therefore, MDS1 is also indispensable for the effective conversion of DBT to environmentally benign CS_2 and other valuable sulfur-free products.

3.2.2. Active components in MDS1 and MAC1

To rationalize the active components in MDS1 and MAC1, more control experiments were designed, and the results are shown in Table S6 and Fig. 1(c). Entry 1-O corresponds to a control experiment using the MDS1-O catalyst, which is the oxide form of MDS1. The product distribution in entry 1-O is similar to that in entry 4 but distinctly different from that in entry 1, suggesting that the sulfide-form catalyst MDS1 cannot be replaced by an oxide-form counterpart. This phenomenon can be because appropriate active sites for desulfurization, which are widely reported as sulfur vacancies, only exist on the surface of sulfide-form catalysts [42]. To investigate the function of metals in

MAC1, MAC2 (no Ag), MAC3 (no Ce) and MAC4 (no Ga) were evaluated. According to Fig. 1(c), MAC2 and MAC3 lead to similar reactant conversions and product distributions. The yields of desulfurized products such as biphenyl and BTX are similar to those in entry 1, indicating that the desulfurization reaction proceeds smoothly. However, a much lower CS_2 yield is observed in these two entries, suggesting the active roles of Ag and Ce in the formation of CS_2. Moreover, methane conversion and the yields of desulfurized products are extremely limited in entry 1-MAC4, indicating that methane is not fully activated without Ga. The conclusion that Ga is essential for methane activation has also been repeatedly reported in previous work [17,33].

3.2.3. *Reactions with controlled reaction time*

The reaction performances at different reaction times in entry 1 are illustrated in Fig. 1(d). Ethane, biphenyl, high boiling point soluble products and coke can be observed at the very beginning (1 min) of the process, confirming they are the products of primary reactions. Comparing the results in Fig. 1(b) and Fig. 1(d), the methane conversion increases even after 45 min, while the DBT conversion achieves the level under an inert atmosphere (entry 2) in 30 min, implying the methane activation and corresponding catalytic desulfurization are slower than the thermal pyrolysis of DBT. Monocyclic aromatic species (mainly BTX) appear after 30 min, indicating that the decomposition of biphenyl is a relatively slow secondary reaction. The amount of CS_2 reaches a detectable level only after 45 min, which is the latest appearing final product, implying its formation could be a rate-determining step. After 60 min, no significant change in the reactant consumption and product distribution can be further observed, suggesting the reaction equilibrium is achieved. Therefore, 60 min is validated as an appropriate reaction time for this MDS process. These results are also consistent with the mass spectra of gas products (Fig. S5). Hydrogen, methane, ethane and carbon disulfide are detected as the major gas-phase products as indicated in Fig. S5(f). No significant peak at the mass value of 34 can be observed, confirming the absence of H_2S. Although ethane is observed as an immediate product at the reaction time of only 1 min, a much longer time (> 30 min) is needed for the appearance of CS_2.

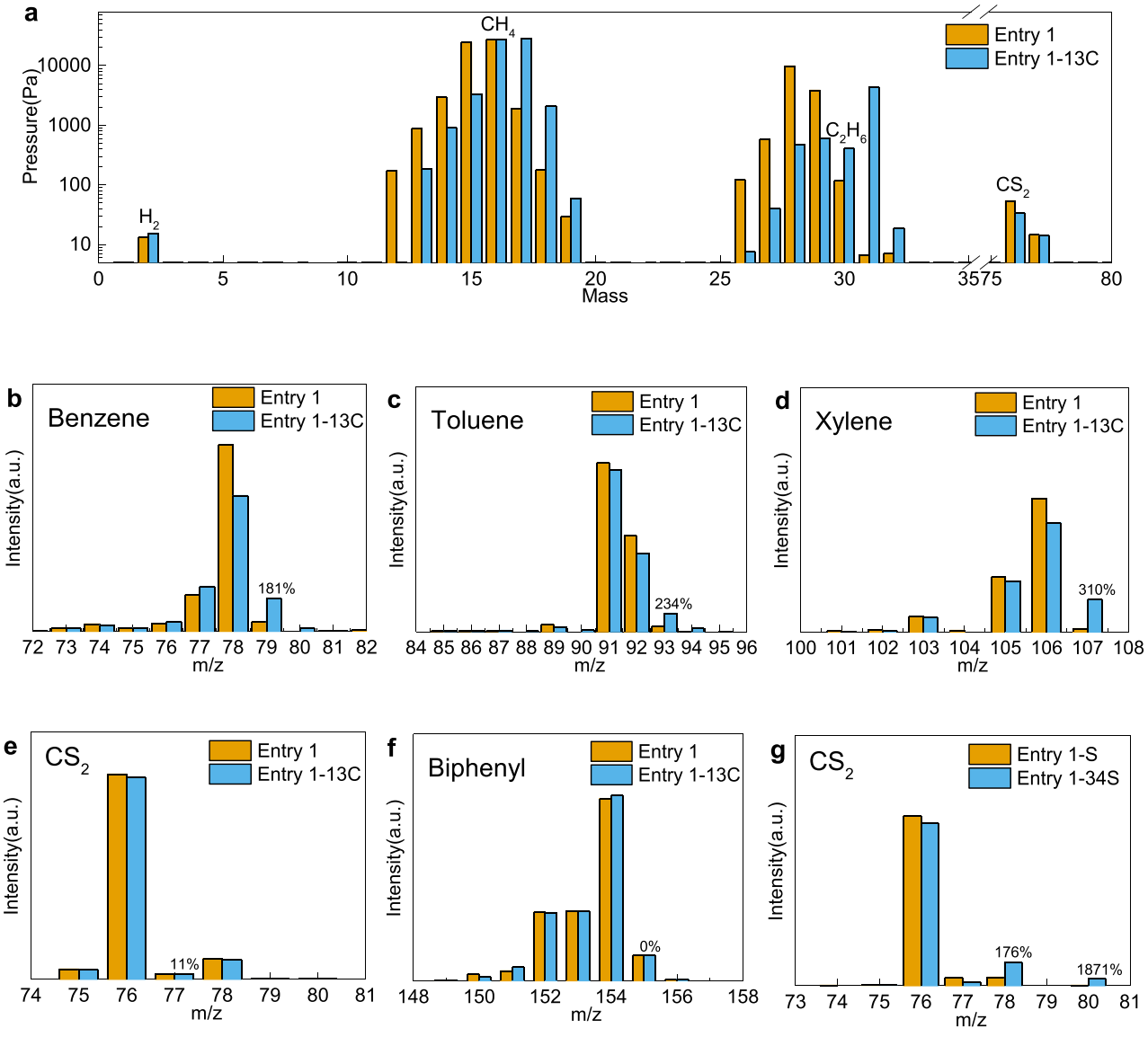

Fig. 2. Mass spectra of isotope labeling experiments. (a) Gas-phase products in ^{13}C isotope labeling experiment. The main peaks of major products are indicated and no intensively overlapped peaks are observed. (b~f) Benzene, toluene, xylene, carbon disulfide and biphenyl in ^{13}C isotope labeling experiment. (g) Carbon disulfide in ^{34}S isotope labeling experiment. The numbers above the column indicate the increasing degree of signal intensities in isotope-labeled entry compared to those in the entry with natural isotope abundance.

3.3. Isotope labeling experiments

3.3.1. ^{13}C isotope labeling

To determine the evolution of carbon atoms in the reaction process, an isotope labeling reaction, labeled as entry 1–13 C, was carried out using ^{13}C-concentrated methane. The mass spectra of gas products in entries 1 and 1–13 C were obtained by a residual gas analyzer (RGA) and are shown in Fig. 2(a). No peak at mass value= 34 can be observed, confirming the absence of H_2S in the products. Besides the expected peak of ^{13}C labeled methane, an apparent peak shift to a higher mass value can be observed for ethane, suggesting that ethane is mainly generated from methane. However, no such peak shift is notably observed for CS_2, implying the carbon atom in CS_2 is not fully derived from methane. The soluble product was analyzed by gas chromatography-mass spectrometry (GC-MS) and ^{13}C nuclear magnetic resonance (NMR) spectroscopy, and the results are illustrated in Fig. 2 (b~f), Fig. S6 and Table S7. According to the mass spectra in Fig. 2 (b~d), the distributions of *m/z* for monocyclic aromatic products clearly shift to higher values for entry 1–13 C compared to those in entry 1, indicating methane incorporation in these products. The degree of signal increase follows the order xylene (310%) > toluene (234%) > benzene (181%), suggesting that the ^{13}C atoms from $^{13}CH_4$ are incorporated preferably on the side chain as methyl groups rather than in the aromatic ring. This conclusion is further supported by the ^{13}C NMR analysis in Fig. S6. However, the degree of signal increase of CS_2 is only 11%, implying that the carbon atom in CS_2 is not fully from methane (Fig. 2 (e)), coinciding with the gas-phase results in Fig. 2(a). Moreover, no signal increase is observed for biphenyl, indicating that the carbon

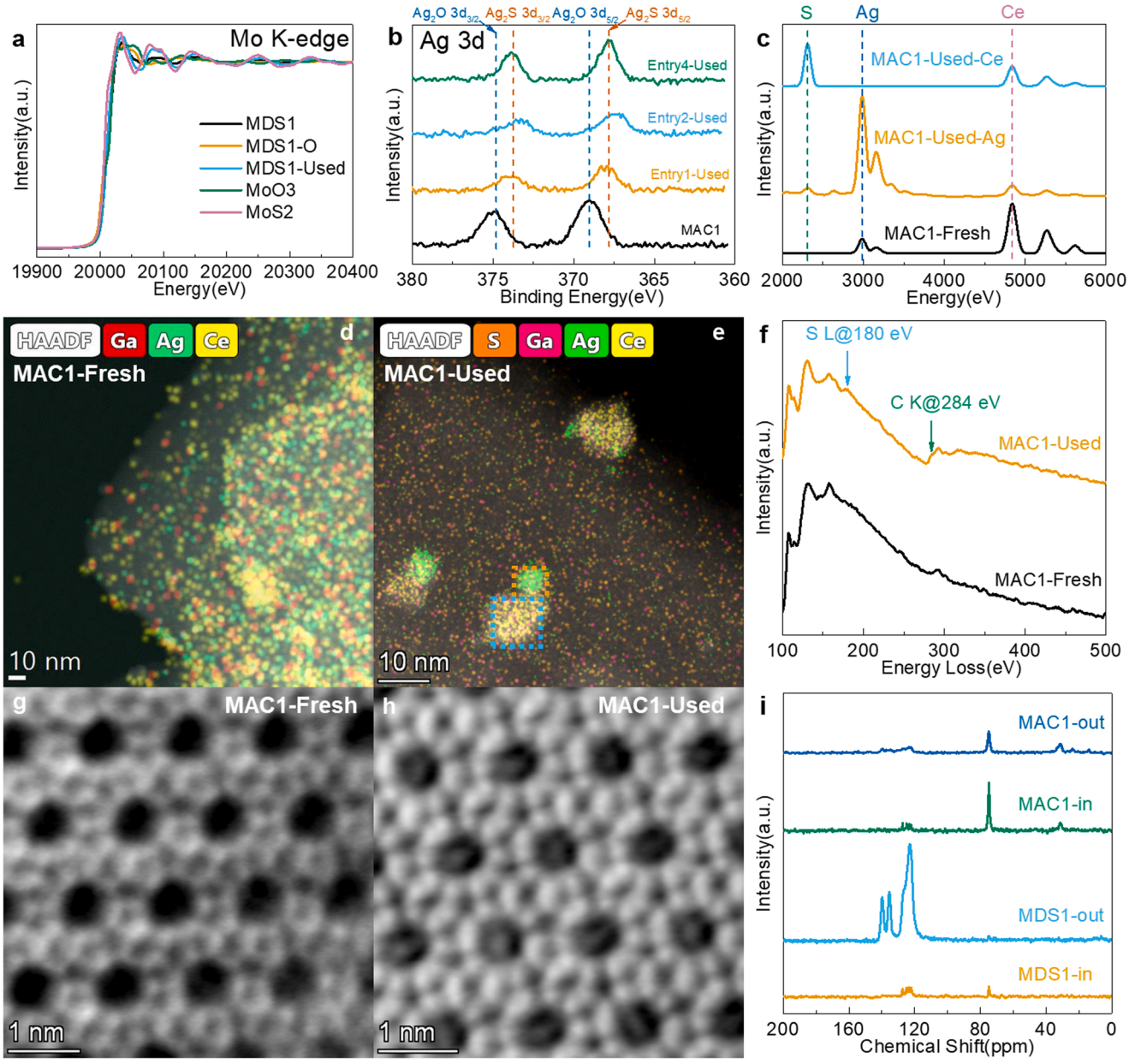

Fig. 3. Catalyst characterizations. (a) Mo K-edge XAFS spectra of fresh and used MDS1 catalysts, MDS1-O catalyst and standard samples. (b) XPS spectra of fresh and used MAC1 catalysts. (c) EDX spectra of fresh and used MAC1 catalysts. The appearance of the S peak can be observed in both Ag rich area (orange frame in Fig. 3(e)) and Ce rich area (blue frame in Fig. 3(e)) of the used catalysts. (d, e) EDX mapping of fresh and used MAC1 catalysts. (f) EELS of fresh and used MAC1 catalysts. (g, h) High-resolution STEM-iDPC images of fresh and used MAC1 catalysts. (i) $^{13}C\{^1H\}$ SS CP/MAS NMR of vial-separated MDS1 and MAC1 catalysts after the reaction. It is observed that aromatic species (120–140 ppm) are preferably adsorbed over MDS1 and alkyl groups (25–35 ppm) are present over MAC1. (For interpretation of the references to color in this figure legend, the reader is referred to the web version of this article.)

atoms in biphenyl almost come entirely from DBT (Fig. 2(f)). This unique ^{13}C distribution provides additional insight into the reaction mechanism. The liquid ^{13}C NMR spectra of soluble products in entry 1 and entry 1–13 C are shown in Fig. S6 and the peak areas are compared in Table S7. The results in Table S7 further confirm the incorporation of the C atom from methane into the soluble products. The different ratio of alkyl and aromatic ^{13}C peak area in entry 1 and entry 1–13 C indicates that methane incorporates preferably as a side chain alkyl group, which is also consistent with our previous studies regarding the catalytic upgrading process under a methane environment [28,31,33,43].

3.3.2. ^{34}S isotope labeling

To substantiate the important role of the sulfide catalyst in the MDS process, the reactions described in entry 1-S and entry 1–34 S were carried out using the MDS1 catalyst derived from natural elemental S and ^{34}S, respectively. According to Fig. 2(g), the intensity ratios at *m/z* 78/76 (0.049) and 80/78 (0.042) for CS_2 in entry 1-S agree well with natural sulfur isotope abundance (^{34}S:^{32}S=0.043). However, it is clear that the intensities at *m/z* 78 and 80 (corresponding to $C^{32}S^{34}S$ and $C^{34}S_2$) dramatically increase in entry 1–34 S, indicating the incorporation of S atoms from the catalyst in the final CS_2 product, which can be attributed to the sulfur exchange between the ^{32}S captured from DBT and the ^{34}S initially present in the isotope-labeled catalyst. This sulfur exchange has also been reported as a critical step of the HDS process in previous studies [44,45].

3.4. Catalyst characterizations

3.4.1. XAFS

The sulfur-capturing capability of MDS1 was further confirmed by X-ray adsorption fine structure (XAFS) analysis as shown in Fig. 3(a) and Fig. S7. According to Fig. 3(a), the patterns of the Mo K-edge in sample MDS1-O are similar to those in the MoO_3 standard, confirming the oxide nature of this catalyst. However, the features in MDS1 seem to be a combination of MoO_3 and MoS_2. Further quantification results in Table S8 also confirm that both Mo-O and Mo-S bonds can be observed in MDS1, indicating the sample might have been partially oxidized during the measurement after inevitably exposed to air for a considerable period. This result can be attributed to the tendency of MDS1 towards being oxidized with exposure to air, which is also consistent with the decrease of sulfur content in the catalyst along with storage time (the sulfur content in MDS1 decreases from 7.35 to 5.75 wt% after storage for one month). The coordination number of Mo-S is much lower than the theoretical value of 6, which is possibly caused by the presence of sulfur vacancies and the imperfect morphology of MoS_2. The conclusion is further supported by STEM results in the following part. In contrast, MDS1-O is in pure oxide form without a Mo-S bond, which is proven to be stable under an ambient environment. However, it is worth noting that the used catalyst MDS1-Used is in pure sulfide form and the coordination number of Mo-S increases significantly, proving that sulfur from the reactant has been captured by the sulfur vacancies of the charged catalyst during the reaction process. This occurrence further confirms the participation of the MDS1 catalyst in the desulfurization reaction and the importance of sulfur vacancies for desulfurization activity. Similar conclusions can be drawn from the Ni K-edge and S K-edge spectra. Both Ni-O and Ni-S bonds can be observed in MDS1 (Fig. S7(b) and Table S9), suggesting that the catalyst is partially oxidized. Again, MDS1-O is proved to be in pure oxide form without a Ni-S bond. For S K-edge XANES in Fig. S7(c), it is observed that MDS1 has been oxidized to sulfate while MDS1-Used mainly maintains in sulfide form, indicating the catalyst was further sulfurized after the reaction.

3.4.2. XRD

The XRD patterns of several typical catalyst samples are shown in Fig. S8. In general, three types of crystalline peaks are observed. The first type of peak located at $2\theta = 25^\circ$ belongs to the TiO_2 crystal structure, and is thus present in all catalysts which contain TiO_2 support (MDS1, MDS1-O and corresponding used catalysts). The second type is a series of typical zeolite diffraction peaks widely distributed from $2\theta = 8^\circ$ to $2\theta = 83^\circ$, which is presented in all catalysts containing ZSM-5 support (MAC1 and corresponding used catalysts). The third type contains sharp peaks at $2\theta = 11^\circ$ and $2\theta = 28^\circ$, which belong to unconverted DBT. However, no peaks for metal clusters or corresponding oxide/sulfide of active components are clearly witnessed, indicating their presence as well dispersed particles with a size smaller than the detection limit of the XRD technique (c.a. 4 nm) or the amorphous nature of corresponding phases.

3.4.3. XPS

The XPS spectra of several elements in MDS1, MAC1 and corresponding used catalysts are shown in Fig. 3(b) and Fig. S9. The X-ray photoelectron spectroscopy (XPS) results in Fig. 3(b) clearly suggest that the Ag in MAC1-Used is sulfurized. This observation can be due to the high affinity of S to Ag atoms, which might lead to the sulfur transfer between MDS1 and MAC1 catalysts. This sulfur transfer process might be responsible for the formation of the new sulfur-containing product CS_2 and is further discussed in the following section based on the results of confirmation experiments. From Mo 3d signal in Fig. S9(a), the peak of molybdenum oxide and molybdenum sulfide can be clearly differentiated. MDS1 and related used catalysts mainly contain MoS_2. However, the peak of MoO_3 is also observable, which indicates that the catalysts might have been partially oxidized with the exposure to air, agreeing with the EXAFS results. MDS1-O only has characteristic peaks of molybdenum oxide. Considering the low desulfurization activity (Table S6 and Fig. 1(b)), the necessity of Mo in sulfide rather than oxide form for successful desulfurization is further confirmed. This conclusion is also clearly substantiated by S 2p signals (Fig. S9(b)), in which the characteristic peaks of sulfide are absent in oxide form catalyst MDS1-O. According to the Ce 3p signals (Fig. S9(d)), the chemical environment of Ce keeps almost unchanged during the reaction process, which is supported by the similar peak patterns in all relevant catalysts. Unfortunately, no detectable peaks can be found in Ni 2p and Ga 3d regions (Fig. S9(e, f)), which might be due to their low content (~1 wt%) and surface abundancy in the prepared catalyst.

3.4.4. STEM

Comprehensive STEM characterizations are performed and shown in Fig. 3~5 and S10~S15. The energy-dispersive X-ray spectroscopy (EDX) mapping results validate the coexistences of Ag-S and Ce-S in MAC1-Used (Fig. 3(c~e) and Fig. S14(b)). The sulfidation of Ag is confirmed by EXAFS and XPS results above, which results in the transfer of sulfur from MDS1 to MAC1 catalyst. Meanwhile, according to the results in Table S6 and Fig. 1(b), Ce is also responsible for the facilitation of sulfur transfer. This effect might be explained by the electron transfer capability of the generated oxygen vacancies over CeO_2, which has been reported in previous work [46]. Therefore, although desulfurization occurs primarily over MDS1, a sulfur transfer process from MDS1 to MAC1 also takes place with the assistance of Ag and Ce during the reaction.

To verify the formation of CS_2, high-angle annular dark-field (HAADF) scanning/transmission electron microscopy (STEM) was used. To visualize the beam-sensitive porous structure of the zeolite ZSM-5 and identify the chemical compositions of the absorbents in MAC1, an integrated differential phase contrast (iDPC) STEM technique was employed to image the fresh and used MAC1 catalysts. The framework of ZSM-5 is clearly seen from the [010] projection with atomic resolution in Fig. 3(g~h), and these results are in good agreement with the theoretical model and previous TEM work [47]. In contrast to the empty channels of the fresh catalyst in Fig. 3(g), the channels of the used catalyst are almost fully occupied by light-absorbent molecules. The carbon and sulfur signals can be clearly identified in both integrated STEM-electron energy loss spectroscopy (EELS, Fig. 3(f)) and EDX

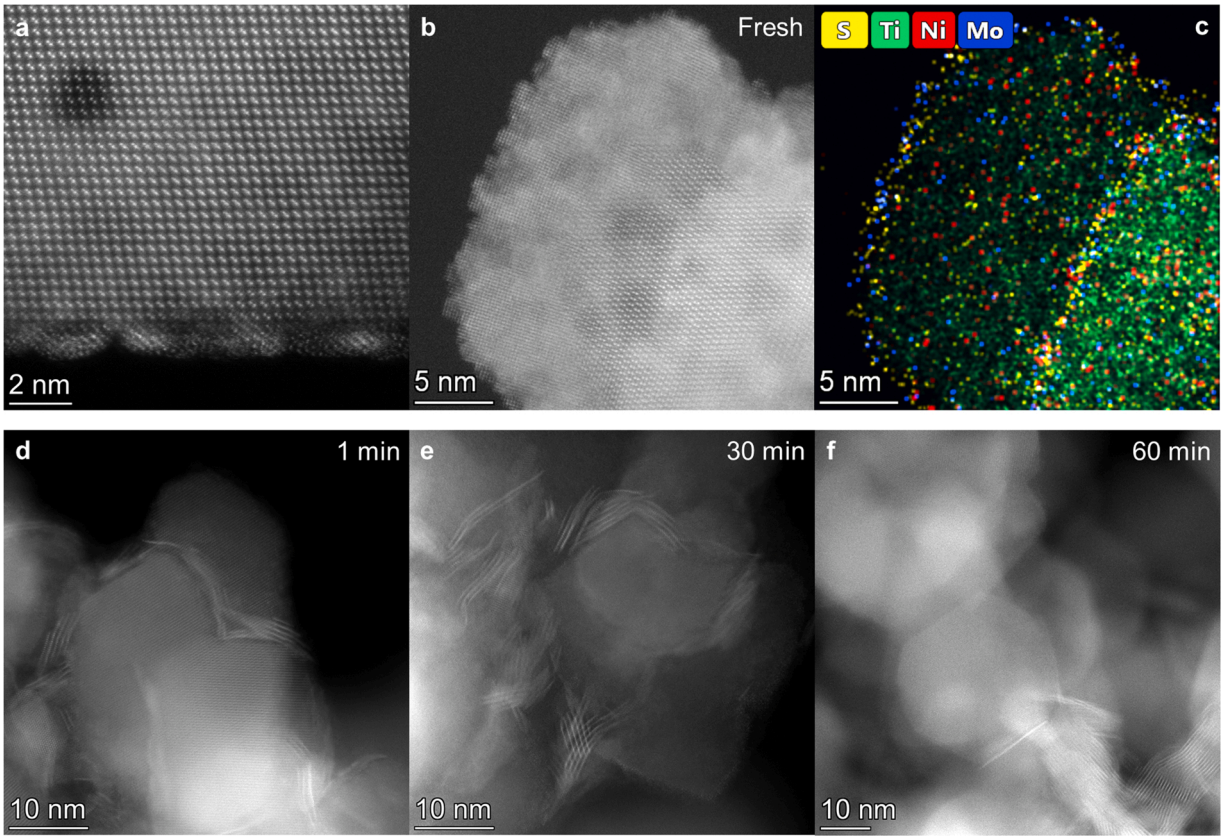

Fig. 4. STEM characterizations of fresh MDS1 catalyst and used MDS1 catalysts with controlled reaction times. (a~c) HAADF-STEM images and EDX mapping results of fresh MDS1 catalyst, showing the metal sulfide in the form of nanoparticles. (d~f) HAADF-STEM images of used MDS1 catalysts after the reaction for 1 min, 30 min and 60 min, respectively, indicating layered structures of metal sulfide are formed during the reaction.

spectra (Fig. S15(c)), which were collected from the ZSM-5 areas without sulfurized Ag or Ce compounds (Fig. S15(a~b)). These observations suggest that the absorbent molecules are carbon-sulfur compounds, implying that CS_2 might be formed and the process occurs preferably over MAC1. Although CS_2 is hardly survived over the catalyst due to its high volatility, the possibility of its presence in the porous structure of ZSM-5 can be significantly increased due to the strong capability of microporous materials to trap volatile molecules even after an evacuation process, which has been reported in previous work [48].

The used catalysts for the reactions with controlled reaction times were also comprehensively characterized as shown in Figs. 4 and 5. According to Fig. 4(d), the layered structure of metal sulfide is clearly observed only after the reaction time of 1 min, which is maintained in used catalysts with longer reaction times (Fig. 4(e, f)), indicating that the structure change of metal sulfide from nanoparticles (Fig. 4(a~c)) to the layered structure is a relatively fast process. However, since fresh MDS1 catalyst is also treated thermally in the preparation process under inert gas while the layered structure is not fully constructed as shown in Fig. 4(a), it can be concluded that the structure change is triggered in the presence of reactants. Interestingly, sulfur is already observed in the used MAC1 catalyst only after the reaction time of 1 min as shown in Fig. 5(a, d). Therefore, the surface sulfur transfer from the MDS1 catalyst to the MAC1 catalyst is also relatively fast. Considering the abundance of S in the MDS1 catalyst which is in sulfide form, it is highly possible that the S atoms originally in MDS1 contribute to the fast sulfur transfer, which occurs together with the structure change of sulfide in MDS1 simultaneously. The sulfur content in MAC1 continues to increase along with reaction time as illustrated in Fig. 5(b~e), which can be due to the further conversion of DBT and the transfer of subsequently generated S atoms, coinciding with the product distribution in Fig. 1(d). It should be noted that since the S atoms over MAC1 are present at the very early stage of the reaction, the absence of sulfur should not be the reason for the late emergence of CS_2. Looking back to Fig. 1(d), the increase of methane conversion is relatively slow during the process. According to the mechanism in Fig. 1(a), the activated methane is responsible for triggering a series of reactions including the hydrogen transfer reaction to form carbon atoms over the catalyst surface, it is highly possible that the formation of CS_2 is limited by the rate of methane activation.

The results of microstructural analysis of molybdenum sulfide in the fresh and used MDS1 catalysts are further shown in Figs. S10–S13. The mapping results of fresh MDS1 (Fig. S10(h)) indicate the dispersions of Mo, Ni and S over TiO_2 support are not identical. A similar distribution of Mo and S can be observed, indicating the presence of MoS_x species. These species are widely present in the form of nanoparticles as shown in Fig. S11. Ni is distributed unevenly, which may or may not be present in MoS_x species. These (Ni)MoS_x nanoparticles possess abundant sulfur vacancies as proved by XAFS results (Tables S8 and S9), which are regarded as the active sites for direct desulfurization of DBT. Fig. S12(f) shows the (Ni)MoS_x species as a layered structure in the used MDS1 catalyst. This construction of the structure containing one to three layers of metal sulfide is widely observed as shown in Fig. S13, which is consistent with the increased sulfur content and coordination number of Mo-S in used MDS1 compared to those in the fresh one and is also proved by sulfur content measurement (7.35 wt% in fresh MDS1 and 11.91 wt% in used MDS1) and EXAFS results (Fig. S7), respectively. According to the EDX mapping results in Fig. S10(c), the dispersions of Ag, Ga and Ce in fresh MAC1 are also proved to be different: Ag is dispersed as small nanoparticles over ZSM-5 support; Ga is atomically dispersed in the inner pores of the support; Ce tends to form nanoparticles on the surface of the support. Fig. S12(c) demonstrates the dispersion of Ag, Ga and Ce in the used MAC1 catalyst. It can be seen that Ga remains well dispersed in the internal pores of ZSM-5 support, while agglomeration of Ag and

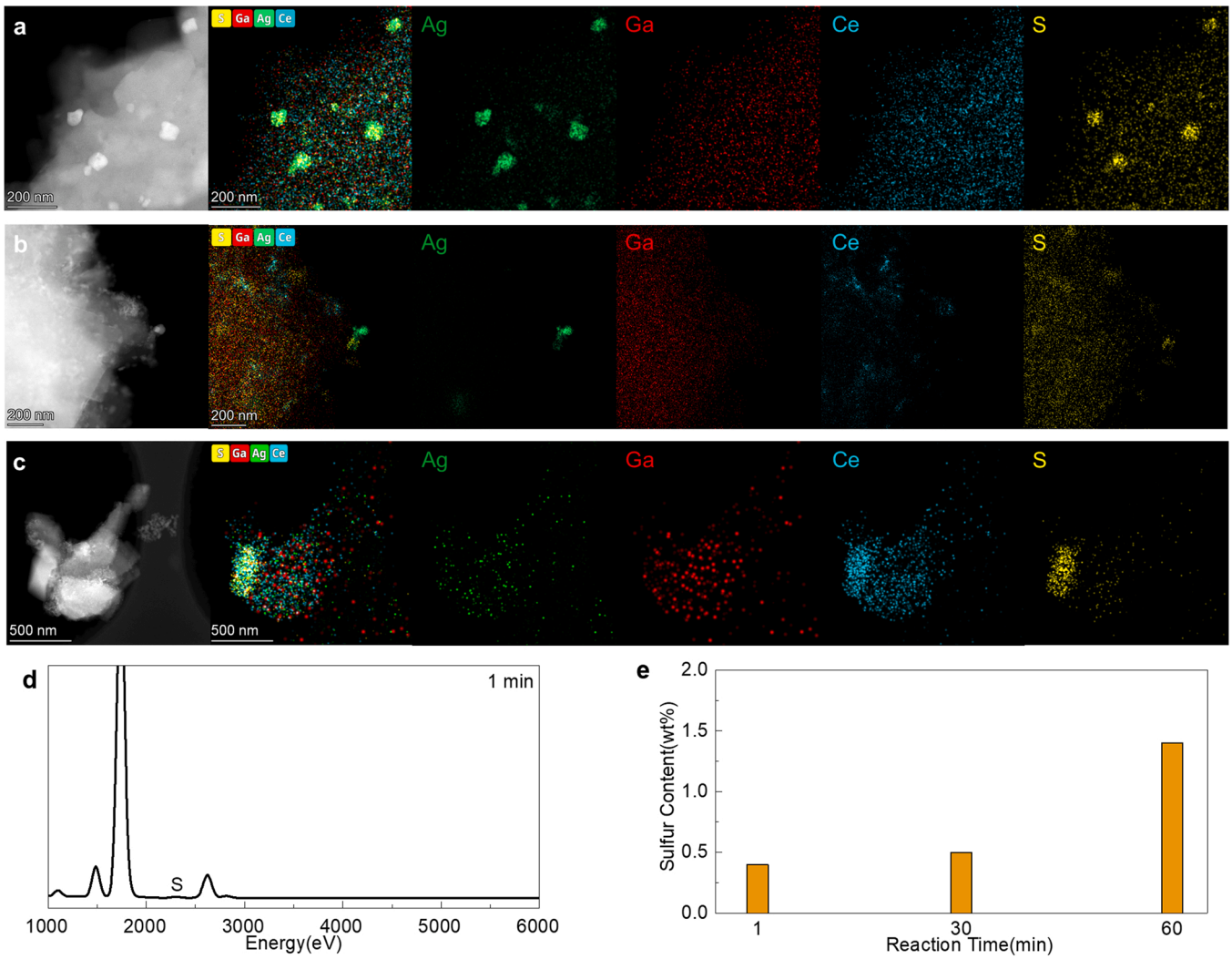

Fig. 5. STEM characterizations of fresh MAC1 catalyst and used MAC1 catalysts with controlled reaction times. (a~c) HAADF-STEM images and EDX mapping results of used MAC1 catalysts after the reaction for 1 min, 30 min and 60 min, respectively. The sulfur is clearly observed with high proximity to silver after the reaction for only 1 min. (d) EDX spectra of used MAC1 catalyst after 1-minute reaction, further confirming the presence of sulfur. (e) The sulfur content in used MAC1 catalysts with different reaction times quantified by EDX spectra. Considerable sulfur content is observed in the used MAC1 catalyst after the reaction for only 1 min, and the value is increasing along with time in the whole reaction process.

Ce can be observed.

3.4.5. SS NMR

$^{13}C\{^{1}H\}$ CP MAS NMR spectra of several used catalytic with controlled reaction times are shown in Fig. S16. The peak located at 75 ppm can be attributed to residual solvent 1,1,2,2-tetrachloroethane used for extraction. The typical peaks of aromatics with the chemical shifts from 120 to 150 ppm can be clearly seen over all used catalysts, which can be due to the adsorption of unreacted DBT. However, the wide peak becomes narrower over catalyst used for 60 min, implying the presence of well-ordered small monocyclic aromatic species such as benzene, toluene and xylenes. The changes are late due to the relatively low rate of biphenyl decomposition as shown in Fig. 1(d). Besides, alkyl peaks with chemical shifts from 25 to 35 ppm, which can be generated after methane activation and alkylation of aromatic species, are becoming increasingly significant along with the reaction process until 60 min. This observation confirms again that methane activation proceeds relatively slowly during the reaction, which controls the formation of methyl-substituted aromatic products and carbon disulfide.

3.5. Mechanism study

3.5.1. Vial-separated catalyst components

It has been proved that MDS1 and MAC1 are both indispensable components for DBT desulfurization under a methane environment. In order to further distinguish the different functions of MDS1 and MAC1 in the reaction network, control experiments were carried out using vial-separated MDS1 and MAC1 catalysts and the results are shown in Table S10. No significant difference in gas product ethane is observed, indicating that the activation of methane is not interfered with by separating two catalyst components. However, as the most important liquid product, no CS_2 is detected in entry MDS1 +DBT|MAC1 or MAC1 +DBT|MDS1, neither inside nor outside the vial. The absence of CS_2 in the two confirmation experiments with vial-separated catalyst components clearly indicates that sulfur transfer over the surface of catalysts is indispensable for CS_2 formation. Besides, it is observed that the yields of BTX and biphenyl are higher over MDS1 than over MAC1, while the yields of other aromatics (and coke) are higher over MAC1 than over MDS1. This result may suggest that DBT desulfurization and biphenyl decomposition towards benzene, toluene and xylenes (BTX) mainly occur over MDS1. Then, these products can be transferred to

MAC1 for subsequent reactions to produce higher aromatics (with 9 or more C atoms) through methylation due to the presence of abundant methyl groups. Different from the surface transfer of sulfur, these products are more volatile under given reaction conditions (the boiling points of biphenyl and BTX species are all much lower than the reaction temperature of 400 °C) and a gas phase transfer is thus possible, which explains the fact that these products are present on both catalyst components while CS_2 is absent.

$^{13}C\{^1H\}$ CP MAS NMR spectra of the collected vial separated catalyst samples were also acquired to further substantiate the conclusions as shown in Fig. 3(i). The sharp peak located at 75 ppm can be attributed to residual solvent 1,1,2,2-tetrachloroethane. A series of aromatic peaks with chemical shifts from 120 to 140 ppm can be observed clearly over the MDS1 catalyst. The broader peaks over MDS1-out are suggestive of adsorbed unreacted DBT species. However, narrower peaks are observed in MDS1-in, which suggest the presence of well-ordered small monocyclic aromatic species such as benzene, toluene and xylenes that are not tightly adsorbed. This difference may be explained by the fact that the volume outside the vial (90 mL) is much larger than that inside the vial (10 mL), so that abundant DBT species is present over MDS1-out and cannot be fully converted. In contrast, the small amount of DBT inside the vial can be fully converted into monocyclic aromatics over MDS1-in. It should be noted that the aromatic peaks can also be detected over MAC1-in and MAC1-out, while the intensities are much lower, suggesting DBT prefers to be adsorbed and converted over MDS1 rather than over MAC1 catalyst. Moreover, alkyl peaks with chemical shifts from 25 to 35 ppm are present over the MAC1 catalyst, which can be generated after methane activation and alkylation of aromatic species. These peaks are hardly observed over MDS1, suggesting MAC1 rather than MDS1 is responsible for the generation of alkyl groups and triggering methylation reactions. These qualitative results are consistent with quantitative measurement results in Table S10, which further clarify the function of MDS1 and MAC1 catalyst components during the reaction process.

3.5.2. CH_4 background reaction

To confirm the capability of two catalyst components for methane activation, verification experiments with MDS1 and MAC1 catalyst components were carried out without DBT feedstock under a methane environment and labeled as M1 and M2, respectively. The results are shown in Table S11. It can be concluded that MDS1 is not responsible for methane activation, which is evidenced by the extremely limited amount of gas products. The positive methane conversion of 0.6% might come from experimental error (~1%). However, MAC1 leads to much higher yields of hydrogen and ethane, proving its capability for methane activation. It should be noted that the methane conversion is still limited, which can be due to its intrinsic inertness under the reaction conditions. Moreover, comparing entry M2 and entry 4 (in Table S5), it is observed that methane conversion is higher with the presence of DBT over the same catalyst MAC1, indicating the synergistic effect between DBT and methane in terms of the promotion of methane utilization. This synergy between methane and other hydrocarbons is also widely observed in previous studies [17,32–34,41,43,49].

3.5.3. Biphenyl experiments

As mentioned above, valuable monocyclic aromatic products are generated during the MDS process, which might come from the decomposition of biphenyl. In order to validate the feasibility of the biphenyl decomposition pathway, control experiments with biphenyl as the solid feedstock was designed and the results are shown in Table S12. It is demonstrated that in entry Bph1, the yields of benzene, toluene and xylenes are significant, indicating that the biphenyl decomposition process is going on smoothly with the presence of MDS1. The methyl groups directly connected to the aromatic ring can be derived through an alkylation process after methane is asymmetrically decomposed over a metal-loaded ZSM-5 catalyst, which has been reported in previous work [50]. However, in entry Bph2, the yields of similar products are extremely limited. Therefore, MAC1 is not as helpful as MDS1 for the facilitation of biphenyl decomposition. It can be concluded that the production of monocyclic aromatic products from DBT requires the realization of direct desulfurization and biphenyl decomposition, and MDS1 plays an important role in both two pathways.

3.5.4. Benzene alkylation

To further evaluate the capability of catalyst components MDS1 and MAC1 for methane activation and subsequent alkylation of aromatic products, confirmation experiments using benzene as the liquid feedstock and methane atmosphere were carried out as shown in Table S13. According to the results in entry B1, extremely limited methane and benzene conversion can be observed, which could be fully attributed to experimental error and feedstock impurity, indicating no methane activation and alkylation can be triggered over MDS1. However, the data in entry B2 clearly indicates that methane activation and benzene alkylation do occur with the presence of MAC1 under given reaction conditions. This conclusion is consistent with the ^{13}C isotope labeling experiment and is also widely reported in previous studies [17,33,34,51].

3.5.5. CS_2 experiments

According to the results shown in Table S4 and Fig. 1(a), carbon disulfide is detected as a new sulfur-containing product, which is only present in the MDS process. A subsequent experiment is designed to confirm its stability in the reaction process, i.e., whether it is stable as a final product without subsequent reactions. The results are tabulated in Table S14. In this case, a significant amount of CS_2 is detected in the gas phase, which can be due to its high volatility with a boiling point of only 46 °C. However, in previous runs, the amount of CS_2 in the gas phase is below the detection limit of micro-GC. This can be explained by the limited CS_2 yield and the adsorption of generated CS_2 species on the surface of the catalyst, which cannot escape freely into the gas phase. These adsorbed CS_2 species can be partially extracted after the addition of TCE solvent and is thus present in the final soluble phase. To sum up the unconverted CS_2 in the gas and soluble phase, it can be concluded that at least 76% of CS_2 remains unreacted after the reaction under similar conditions of entry 1. Besides, neither H_2S in the gas phase nor any other sulfur-containing species in the soluble phase is detected. The only detectable products include H_2 and C_2H_6, which might come from methane upon activation as previously indicated in entry 4 and no CS_2 involvement is needed. Therefore, it is highly possible that CS_2 is stable under current reaction conditions, which can survive as the final product in the DBT desulfurization process under methane and is otherwise converted to H_2S under a hydrogen rich atmosphere. The gap between 76% CS_2 recovery and the theoretical value of 100% could be attributed to coke formation and the loss of highly volatile CS_2 during the measurement processes.

3.5.6. Reaction with 4-methylDBT and 4,6-dimethylDBT

After the confirmation of the DBT desulfurization process under a methane environment, it is also interesting to explore the possibility of converting more challenging sulfur-containing organic compounds with a similar structure to DBT. 4-methylDBT and 4,6-dimethyl DBT are two typical derivatives of DBT. 4-methylDBT has one methyl group attached to the aromatic ring next to the sulfur atom in DBT, and 4,6-dimethylDBT has two such methyl groups. The presence of the methyl group generally causes the steric effect, which brings great challenges to the successful removal of the sulfur atom from DBT, especially through the DDS pathway. The corresponding results using 4-methylDBT and 4,6-dimethylDBT as solid feedstocks are listed in Table S15. Comparing these results with those in entry 1, a conversion sequence of DBT > 4-methlyDBT > 4,6-dimethylDBT is observed, and the yields of CS_2 and other aromatic products also decrease dramatically in the same order, indicating that the presence of methyl group significantly inhibits the

removal of the sulfur atom from DBT structure. This phenomenon again confirms that the reaction should follow the DDS pathway, in which the direct anchoring of sulfur atom on the catalytic active site is crucial as the first step. However, the yield of high boiling point soluble products and coke remains at a similar or even higher extent, suggesting the alkylation and polymerization processes are not inhibited but even promoted with the presence of side-chain methyl substituents.

3.5.7. Reaction over MAC1-S

According to the previously discussed experimental results, CS_2 cannot be formed if MDS1 and MAC1 catalyst components are separated by an open mouth vial (Table S10), suggesting CS_2 should be generated over MAC1 catalyst after an essential surface sulfur transfer process, which is also proved by XPS and STEM results. To further elucidate the CS_2 formation pathway, experiments were carried out over sulfurized MAC1-S catalyst with the presence of methane, methane + biphenyl, biphenyl (N_2 atmosphere) and methane + benzene (biphenyl is the desulfurization product of DBT, and benzene is one of the decomposition product of biphenyl). The results are listed in Table S16. It can be clearly seen that CS_2 can be successfully formed even with the absence of MDS1 as long as MAC1 is pre-sulfurized, strongly proving the feasibility of CS_2 generation during the DBT desulfurization process if sulfur can be transferred from MDS1 to MAC1. Interestingly, the amount of produced CS_2 in the liquid product varies significantly in four experiments: high CS_2 yield can be observed in entry MAC1-S1 (CH_4 + biphenyl); lower but non-negligible yield is found in entry MAC-S2 (CH_4 alone); while the yield is limited in entry MAC1-S3 (N_2 + biphenyl) and entry MAC1-S4 (CH_4 + benzene). This observation suggests that CH_4 is essential for triggering the CS_2 formation pathway as an initiator, while the carbon from biphenyl can also take part in the process, leading to the synergy between CH_4 and biphenyl. The contribution of biphenyl to the final product is also further confirmed by the ^{13}C isotope labeling experiment as shown in Fig. S17. The mass spectra of gaseous products in entry MAC1-S1–13 C confirm the existence of both $^{12}CS_2$ (mass=76) and $^{13}CS_2$ (mass=77), while the concentration of $^{12}CS_2$ is much higher. Similar results can be observed in the mass spectra of CS_2 in the soluble phase. The peak located at $m/z = 77$ does increase if $^{13}CH_4$ is used as the feed gas, however, the majority of CS_2 still contains ^{12}C ($m/z = 76$), indicating the carbon in CS_2 mainly comes from other carbon sources, which is biphenyl in this case. Moreover, according to the results in entry MAC1-S3, methane is detected as a product as indicated by the limited but non-negligible negative conversion, which might come from the ring-opening reaction of biphenyl and explains why a trace amount of CS_2 can be observed. However, although benzene is also an observed product, the addition of benzene does not lead to increased CS_2 yield (entry MAC1-S4). On the contrary, the amount of produced CS_2 is even lower than that in entry MAC1-S2. This can be because the ring-opening reaction of benzene is much less significant than that of biphenyl, which is evidenced by the lower coke yield in entry MAC1-S4 compared to MAC1-S1. In contrast, the alkylation reaction between methane and benzene to form toluene and xylene is still observed, which consumes the activated methane and reduces the CS_2 formation.

It should be noted that the synergy between methane and other hydrocarbons is already widely reported in previous studies [17,32–34, 41,43,49]. In a pioneer work, it is proposed that this synergy can be due to the hydrogen transfer reactions between activated methane and other hydrocarbons, which leads to a higher concentration of hydrocarbon intermediates (e.g. CH_3·) [38]. This work also establishes Ga/ZSM-5 as a typical catalyst for methane activation. In the case of CS_2 formation over MAC1, methane is firstly adsorbed and activated preferably in the internal pores of zeolite structure over Ga active sites. This preference is supported by the atomic dispersion of Ga in the porous structure of MAC1 as shown in STEM images (Fig. S10(c)) as well as previous work, in which direct methane activation over Ga/ZSM-5 catalyst is confirmed to take place in the inner pores [43]. However, the biphenyl molecule could be too big to freely diffuse into the internal pores of ZSM-5 in this step, which explains the extremely low CS_2 yield in entry MAC1-S3. Next, volatile radicals after methane activation including CH_x· and H·could be generated. These species can be easily transferred to the surface of the MAC1 catalyst, where it initiates hydrogen transfer reactions with other adsorbed hydrocarbon species derived from co-fed reactant, generating C atoms over the catalyst surface. These C atoms further react with S atoms to form CS_2. Thanks to the hydrogen transfer process, not only the carbon atoms from methane but also those from biphenyl could get involved in the CS_2 formation pathway, which also coincides with the observation that $^{13}CS_2$ is not significantly concentrated in isotope labeling experiment entry 1–13 C as proved by mass spectra (Fig. 2(d)).

3.5.8. Reaction over MAC1 @Si

To confirm the necessity of surface carbonaceous species over MAC1 for the formation of CS_2, a control experiment was performed in which MAC1 was replaced by silica-coated MAC1 (MAC1 @Si). The results are compared with entry 1 (main entry) in Table S17. The methane conversion, H_2 yield and C_2H_6 yield are slightly increased after the silica coating treatment of the catalyst. This might be due to the better methane adsorption capability over the catalyst since a non-polar surface is formed by silica coating. Similar DBT conversion can be maintained, while the coke yield decreases significantly since the surface acidity is decreased and the coking process over the acidic active sites is inhibited, indicating much less active carbon species are present over MAC1 @Si during the reaction. This conclusion is further confirmed by XPS spectra as shown in Fig. S18. It can be seen that the carbon peak intensity is lower over used MDS1 + MAC1 @Si catalysts than that over used MDS1 + MAC1. As a result, no CS_2 can be found as a soluble product, indicating that the surface reaction between active C and S atoms on the external surface of MAC1 is crucial for CS_2 formation. Besides, the yield of other products including biphenyl, other aromatics and high boiling point soluble products are higher after the catalyst is coated by silica. This can also be attributed to better methane activation over the treated catalyst.

3.6. DFT study

3.6.1. Adsorption of reactants on MDS1 and MAC1 catalyst components

The adsorption of two reactants, i.e. methane and DBT, over MDS1 and MAC1 catalyst components were further simulated by the DFT study and the results are shown in Fig. 6(a~b). It can be seen that methane prefers to be adsorbed in the internal pore of the MAC1 catalyst evidenced by the higher adsorption energy (76.2 kJ mol^{-1}), while the adsorption of DBT over MAC1 is highly thermodynamically unfavorable (E_{ads}=−216.8 kJ mol^{-1}), which can be mainly due to the steric effect. On the contrary, MDS1 demonstrates a strong capability for DBT adsorption with the adsorption energy of 55.2 kJ mol^{-1}. Therefore, it is concluded that DBT is adsorbed over MDS1 and methane tends to be adsorbed over MAC1 during the reaction process. This conclusion is also consistent with the observations of experiments with vial-separated catalyst components as shown in Table S10 and Fig. 3(i).

3.6.2. Adsorption of DBT, 4-methylDBT and 4,6-dimethylDBT

After MDS1 is confirmed to adsorb DBT and trigger the MDS process, the influence of the side-chain methyl group on DBT is also corroborated by the DFT results. The optimized structures of adsorbed DBT, 4-methylDBT and 4,6-dimethylDBT are shown in Fig. 6(c), with the adsorption energies of 55.2, 54.0, 51.8 kJ mol^{-1} respectively. The decreasing adsorption energy indicates that the presence of the methyl group leads to weaker adsorption, which is unfavorable for the desulfurization process. This conclusion is also evidenced by the Mo-S_{DBT} (the S atom from DBT) bond length of 4.71, 5.27 and 5.92 angstrom upon adsorption of DBT, 4-methylDBT and 4,6-dimethylDBT onto the MDS1 surface, respectively. This trend coincides well with experimental observations shown in Table S15, which also supports that the DDS rather than HYD

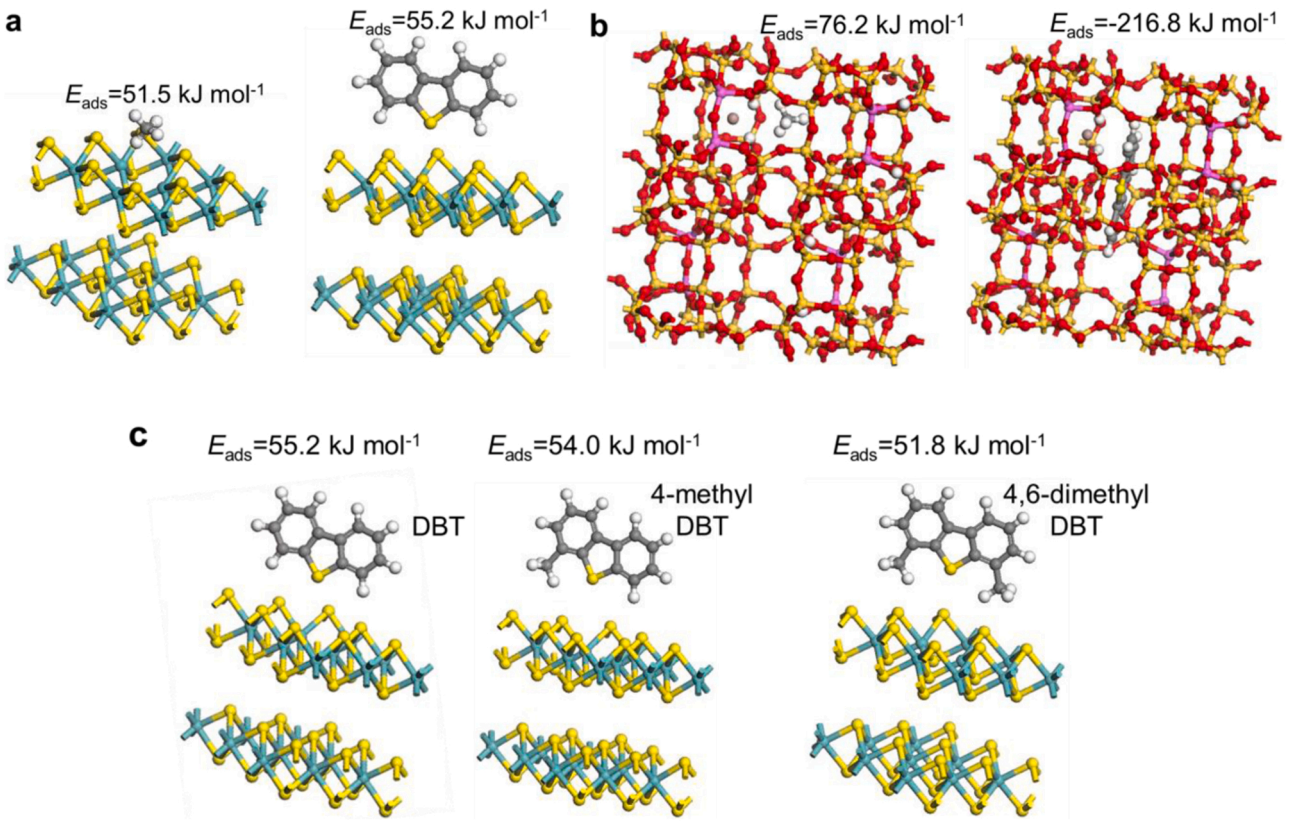

Fig. 6. DFT calculations. (a) Optimized structures and adsorption energies of adsorbed methane and DBT on the sulfur vacancy of MoS_2. (b) Optimized structures and adsorption energies of adsorbed methane and DBT in the inner pore of Ga/ZSM-5. (c) Optimized structures of adsorbed DBT, 4-methylDBT and 4,6-dimethylDBT on the sulfur vacancy of MoS_2. The adsorption energies decrease in the order DBT > 4-methylDBT > 4,6-dimethylDBT, which is consistent with experimental results (Table S15), supporting the DDS pathway.

Table 1
Desulfurization performance of three typical real-world samples in a batch reactor. MDO, RDO, HCO and CN stand for marine diesel oil, renewable diesel oil, heavy crude oil and coker naphtha, respectively.

Entry	Gas	Catalyst	Sulfur content in feedstock (ppm)	Sulfur content in product (ppm)	Desulfurization degree (%)
MDO	32 bar CH_4, 3 bar N_2	MAC1 +MDS1	867 ± 8	588 ± 4	32.2
RDO	32 bar CH_4, 3 bar N_2	MAC1 +MDS1	836 ± 56	370 ± 4	55.7
HCO	32 bar CH_4, 3 bar N_2	MAC1 +MDS1	30,600 ± 500	11,975 ± 59	60.9
CN	32 bar CH_4, 3 bar N_2	MAC1 +MDS1	10,338 ± 484	200 ± 4	98.1

pathway is followed in the reaction process.

3.7. Practical potential: desulfurization of real-world samples

To illustrate the practical potential of the MDS process on real-world samples, several sulfur-containing feedstocks including marine diesel oil, renewable diesel oil, coker naphtha and heavy crude oil, were treated, and the desulfurization performances are shown in Table 1. Successful desulfurization was realized for all samples, with up to a 98.1% desulfurization degree of coker naphtha, in which thiophene is detected as an existing sulfur-containing component (Fig. S19), indicating the versatility of the technique. The molar ratio of methane to removed sulfur atoms is estimated to be 250:1 for the DBT model compound study and 600:1 for the real-world sample (coker naphtha), respectively. The results are similar to the molar ratio of hydrogen to removed sulfur atoms in a typical HDS process (370:1), indicating a comparable molecular efficiency of MDS and HDS processes [6]. It should be noted that although the sulfur content in the above-obtained products still cannot meet the stringent fuel specifications, this method provides an opportunity as a pre-treatment step for oil desulfurization prior to the traditional HDS process, which could help to significantly decrease the demand for hydrogen resources. The mass spectra of volatile liquid products from the heavy crude oil upgrading process are shown in Fig. S20(a). The data were further deconvoluted and simulated

Table 2
Control experiments for desulfurization of coker naphtha (CN). In entry CN-SiC, the catalyst is replaced by unreactive solid silicon carbide. In entry CN-N_2, only inert nitrogen is introduced as the gas atmosphere.

Entry	Gas	Catalyst	Sulfur content in feedstock (ppm)	Sulfur content in product (ppm)	Desulfurization degree (%)
CN	32 bar CH_4, 3 bar N_2	MAC1 +MDS1	10,338 ± 484	200 ± 4	98.1
CN-SiC	32 bar CH_4, 3 bar N_2	SiC	10,338 ± 484	6980 ± 238	32.5
CN-N_2	35 bar N_2	MAC1 +MDS1	10,338 ± 484	1176 ± 86	88.6

spectra are provided in Fig. S20(b). CS_2 is observed as a volatile liquid component, whose signals in the mass spectra are distinctive and do not overlap with other detectable components, clearly suggesting its formation during the real-world sample treatment process. The composition of gas products is further listed in Table S18. It can be seen that C_2-C_3 hydrocarbons are the main gas products. The content of C_4-C_5 hydrocarbons, whose boiling points are similar with CS_2, is limited. Moreover, an efficient process has been developed for the separation of CS_2 and C_5 hydrocarbons [52]. Therefore, favorable efficiency of separating CS_2 and other gas products can be anticipated. The important roles played by the catalyst and methane in the desulfurization process were further explored through control experiments using coker naphtha as a typical feedstock (Table 2). Comparing entry CN and CN-SiC, it is observed that the desulfurization degree increases dramatically from 32.5% to 98.1% after the addition of the catalyst, indicating most of the sulfur species must be removed with the assistance of a catalyst rather than through a thermal process. Comparing entry CN and CN-N_2, the increased desulfurization degree from 88.6% to 98.1% after methane introduction suggests that the participation of methane in MDS reactions also applies to the sulfur removal of real oil samples. Although the 10% increase of desulfurization under methane than under nitrogen might seem insignificant, it is mostly dealing with the refractory sulfur species such as DBT, which is the most difficult part of the desulfurization work, and the remaining sulfur content under methane (200 ppm) is more than four-fifth lower than that under nitrogen (1176 ppm), greatly improving the added value of the oil product since the 200 ppm sulfur content has a much higher chance than 1176 ppm to fall into the range of low-sulfur content oil according to various regulations. Moreover, a 7-day run in a fixed bed reactor was carried out and the process was proven to have satisfactory long-term stability (Fig. S21). Although fast deactivation is witnessed in the first 12 h, over 50% stabilized desulfurization degree is maintained in the rest period of the evaluation, validating the stability of the process. The fast deactivation stage might be attributed to the elimination of unstable active sites caused by the evolution of sulfur vacancies and the coking effect, and a stabilized catalyst form could be generated afterward. These results for commercial oil samples initially validate the feasibility of this new desulfurization route. A scale-up process in light of the methane-regulated desulfurization technique is in progress and the economic assessment, as well as life-cycle analysis, will be obtained to investigate its potential in real practices.

3.8. Proposed mechanism

Based on all the experimental and theoretical results, a catalytic reaction mechanism was proposed as shown in Fig. 1(a). First, DBT is adsorbed on the sulfur vacancies over MDS1 (supported by Fig. 3(a), 4 (a), and S6, Tables S8 and S9) and methane is activated by Ga over MAC1 (supported by Fig. 3(i) and 4(b) and Table S11). Then, the radicals generated after methane activation interact with DBT over MDS1 through the DDS pathway (supported by Fig. 1(d), 4(c) and Table S15) to form an important sulfur-free product, biphenyl and S atoms (supported by Fig. 1(d), S6 and Table S10). Later, biphenyl participates in a series of reactions including decomposition and alkylation, resulting in the formation of other aromatic products such as BTX (supported by Fig. 1(d), 3 (i) and Table S12). In addition, a surface sulfur transfer process from MDS1 to MAC1 occurs with the assistance of Ag and Ce (supported by Fig. 1(d), 3(b~e) and Table S10). Subsequently, the methyl groups generated over MAC1 further trigger hydrogen transfer reactions and produce C atoms over the catalyst surface, and the latter react with the transferred S atoms to form the final sulfur-containing product CS_2 (supported by Fig. 3(f~h), Tables S14 and S16). It should be noted that a series of side reactions, such as ethane formation (supported by Fig. 1 (d), Table S11), coking (supported by Fig. 1(d), Tables S10–S14), methylation (supported by Tables S10 and S13), methyl exchange and ring expansion-contraction of aromatics (supported by Fig. 2(b~d)) also occur during the process, leading to a more diverse product distribution as shown in Fig. 1(b). These side reactions are omitted from Fig. 1(a) for clarity. It can be seen that methane initiates the reaction pathways and comprehensively participates in the reaction process, ending up in several products including ethane (a large portion), aromatic derivatives (an intermediate portion) and carbon disulfide (a small portion), etc. From this surface reaction network, it is clear that MDS1 and MAC1 are also integral to the successful MDS process, and it is this creative catalyst design that drives methane-assisted DBT desulfurization into reality.

4. Conclusion

A methane-regulated desulfurization process using dibenzothiophene as a model compound is realized over a rationally designed dual catalyst system. The reaction mechanism is investigated and supported by extensive confirmation experiments, product and catalyst characterizations, as well as theoretical calculations. It is suggested that methane initiates a direct desulfurization pathway towards an important desulfurized product biphenyl and is incorporated into the final products including ethane, aromatics and carbon disulfide, to different extents. Two catalysts, whose structures are further tuned during the reaction, are also confirmed to work coordinately for the production of carbon disulfide via surface sulfur exchange and transfer processes. The technical feasibility of the route is verified by the desulfurization practice of real-world samples. This work opens a pathway with economic and environmental advantages for better utilization of natural gas resources and removal of sulfur heteroatoms in crudes with carbon disulfide as a product.

CRediT authorship contribution statement

H. Xu performed the reactions, analyzed the data and wrote the manuscript. H. Xu and Z. Li performed isotope labeling experiments. H. Xu and Y. Li performed the sulfur content measurement of solid and liquid samples. P. He and X. Wen performed the liquid ^{13}C NMR and XPS experiments. L. Chang performed the XAFS characterizations. L. Liu analyzed the XAFS data. B. A. Klein and V. K. Michaelis performed the SS CP/MAS NMR characterizations and analyzed the corresponding data. X. Liu and J. Qi conducted the STEM characterization and analyzed the corresponding data. D. Wu provided technical support for iDPC characterizations. H. Xu and S. Meng performed the DFT calculations. H. Song designed the experiments and administrated the project. X. Liu and H. Song supervised the research. All authors revised the manuscript.

Declaration of Competing Interest

The authors declare that they have no known competing financial interests or personal relationships that could have appeared to influence the work reported in this paper.

Acknowledgments

The authors gratefully acknowledge the financial support from Kara Technologies Inc., Natural Sciences and Engineering Research Council of Canada (NSERC) through collaborative research and development program (CRDPJ/531607-18) and Alliance Grant program (ALLRP/560812-2020), Alberta Innovates (AI 2552 and G2020000355) and New Frontiers in Research Fund (NFRF) (VM). H. Xu acknowledges the technical support from Mr. Jack Jarvis for the operation of the fixed bed reactor. X. Liu acknowledges the financial support from the National Natural Science Foundation of China (Grant Nos. 21872163, 22072090, 21991153, 21991150). The authors also appreciate the technical support from Mr. Hiroaki Matsumoto and Mr. Chaobin Zeng from Hitachi High-Technologies (Shanghai) Co. Ltd, for HR-STEM/Hr-SE characterizations.

Appendix A. Supporting information

Supplementary data associated with this article can be found in the online version at doi:10.1016/j.apcatb.2022.121436.

References

[1] P. Amoatey, H. Omidvarborna, M.S. Baawain, A. Al-Mamun, Emissions and exposure assessments of SO_x, NO_x, PM10/2.5 and trace metals from oil industries: a review study (2000–2018), Process Saf. Environ. Prot. 123 (2019) 215–228.
[2] C.E. Zipper, L. Gilroy, Sulfur dioxide emissions and market effects under the clean air act acid rain program, J. Air Waste Manag. Assoc. 48 (1998) 829–837.
[3] R.T. Yang, A.J. Hernandez-Maldonado, F.H. Yang, Desulfurization of transportation fuels with zeolites under ambient conditions, Science 301 (2003) 79–81.
[4] S. Kumar, V.C. Srivastava, S.M. Nanoti, Extractive desulfurization of gas oils: a perspective review for use in petroleum refineries, Sep. Purif. Rev. 46 (2017) 319–347.
[5] I. Mallidis, S. Despoudi, R. Dekker, E. Iakovou, D. Vlachos, The impact of sulphur limit fuel regulations on maritime supply chain network design, Ann. Oper. Res. 294 (2018) 677–695.
[6] S. Brunet, D. Mey, G. Pérot, C. Bouchy, F. Diehl, On the hydrodesulfurization of FCC gasoline: a review, Appl. Catal. A: Gen. 278 (2005) 143–172.
[7] A. Tanimu, K. Alhooshani, Advanced hydrodesulfurization catalysts: a review of design and synthesis, Energy Fuels 33 (2019) 2810–2838.
[8] R. Xu, L.-C. Chou, W.-H. Zhang, The effect of CO_2 emissions and economic performance on hydrogen-based renewable production in 35 European Countries, Int. J. Hydrog. Energy 44 (2019) 29418–29425.
[9] D. Liu, B. Li, J. Wu, Y. Liu, Sorbents for hydrogen sulfide capture from biogas at low temperature: a review, Environ. Chem. Lett. 18 (2019) 113–128.
[10] M. Lincke, U. Petasch, U. Gaitzsch, A. Tillmann, M. Tietze, F. Niebling, Chemoadsorption for separation of hydrogen sulfide from biogas with iron hydroxide and sulfur recovery, Chem. Eng. Technol. 43 (2020) 1564–1570.
[11] Z. Liang, T. Li, M. Kim, A. Asthagiri, J.F. Weaver, Low-temperature activation of methane on the IrO2(110), Surf., Sci. 356 (2017) 299–303.
[12] C. Davis, BP Bearish on Natural Gas Prices, LNG Exports to 2021, 2019.
[13] C. Díaz-Urrutia, T. Ott, Activation of methane: a selective industrial route to methanesulfonic acid, Science 363 (2019) 1326–1329.
[14] V.A. Roytman, D.A. Singleton, Comment on "activation of methane to CH_3 industrial route to methanesulfonic acid", Science 363 (2019) 1326–1329.
[15] V. Rabarihoela-Rakotovao, S. Brunet, G. Perot, F. Diehl, Effect of H_2S partial pressure on the HDS of dibenzothiophene and 4,6-dimethyldibenzothiophene over sulfided $NiMoP/Al_2O_3$ and $CoMoP/Al_2O_3$ catalysts, Appl. Catal. A: Gen. 306 (2006) 34–44.
[16] C. Zhang, W. Song, G. Sun, L. Xie, L. Wan, J. Wang, K. Li, Synthesis, characterization, and evaluation of activated carbon spheres for removal of dibenzothiophene from model diesel fuel, Ind. Eng. Chem. Res. 53 (2014) 4271–4276.
[17] P. He, R. Gatip, M. Yung, H. Zeng, H. Song, Co-aromatization of olefin and methane over Ag-Ga/ZSM-5 catalyst at low temperature, Appl. Catal. B: Environ. 211 (2017) 275–288.
[18] A. Pines, M.G. Gibby, J.S. Waugh, Proton-enhanced nuclear induction spectroscopy. a method for high resolution nmr of dilute spins in solids, J. Chem. Phys. 56 (1972) 1776–1777.
[19] A.E. Bennett, C.M. Rienstra, M. Auger, K.V. Lakshmi, R.G. Griffin, Heteronuclear decoupling in rotating solids, J. Chem. Phys. 103 (1995) 6951–6958.
[20] B. Ravel, M. Newville, Athena, Artemis, Hephaestus: data analysis for X-ray absorption spectroscopy using IFEFFIT, J. Synchrotron Rad. 12 (2005) 537–541.
[21] M. Newville, IFEFFIT: interactive XAFS analysis and FEFF fitting, J. Synchrotron Rad. 8 (2001) 322–324.
[22] E. Yucelen, I. Lazic, E.G.T. Bosch, Phase contrast scanning transmission electron microscopy imaging of light and heavy atoms at the limit of contrast and resolution, Sci. Rep. 8 (2018) 2676.
[23] G. Kresse, J. Furthmuller, Efficient iterative schemes for ab initio total-energy calculations using a plane-wave basis set, Phys. Rev. B 54 (1996) 11169–11186.
[24] G. Kresse, D. Joubert, From ultrasoft pseudopotentials to the projector augmented-wave method, Phys. Rev. B 59 (1999) 1758–1775.
[25] J.P. Perdew, K. Burke, M. Ernzerhof, ERRATA-generalized gradient approximation made simple [Phys. Rev. Lett. 77, 3865 (1996)], Phys. Rev. Lett. 78 (1997) 1396.
[26] C. Baerlocher, L.B. McCusker, Database of Zeolite Structures, 2020.
[27] D.H. Olson, G.T. Kokotailo, S.L. Lawton, W.M. Meier, Crystal structure and structure-related properties of ZSM-5, The, J. Phys. Chem. 85 (1981) 2238–2243.
[28] H. Xu, Z. Li, R.L. Pryde, S. Meng, Y. Li, H. Song, Participation of methane in an economically and environmentally favorable catalytic asphaltene upgrading process, Chem. Commun. 56 (2020) 5492–5495.
[29] Z. Varga, T. Szarvas, P. Tétényi, J. Hancsók, T. Ollár, The particular characteristics of the active sites of MoS2, WS2 catalysts in thiophene hydrodesulfurization, Reaction Kinetics, Mech. Catal. 124 (2017) 61–74.
[30] E. Dominguez Garcia, J. Chen, E. Oliviero, L. Oliviero, F. Maugé, New insight into the support effect on HDS catalysts: evidence for the role of Mo-support interaction on the MoS_2 slab morphology, Appl. Catal. B: Environ. 260 (2020).
[31] A. Wang, D. Austin, A. Karmakar, G.M. Bernard, V.K. Michaelis, M.M. Yung, H. Zeng, H. Song, Methane upgrading of acetic acid as a model compound for a biomass-derived liquid over a modified zeolite catalyst, ACS Catal. 7 (2017) 3681–3692.
[32] J. Jarvis, A. Wong, P. He, Q. Li, H. Song, Catalytic aromatization of naphtha under methane environment: effect of surface acidity and metal modification of HZSM-5, Fuel 223 (2018) 211–221.
[33] Q. Li, P. He, J. Jarvis, A. Bhattacharya, X. Mao, A. Wang, G.M. Bernard, V. K. Michaelis, H. Zeng, L. Liu, H. Song, Catalytic co-aromatization of methane and heptane as an alkane model compound over Zn-Ga/ZSM-5: a mechanistic study, Appl. Catal. B: Environ. 236 (2018) 13–24.
[34] Q. Li, F. Zhang, J. Jarvis, P. He, M.M. Yung, A. Wang, K. Zhao, H. Song, Investigation on the light alkanes aromatization over Zn and Ga modified HZSM-5 catalysts in the presence of methane, Fuel 219 (2018) 331–339.
[35] A. Samoc, Dispersion of refractive properties of solvents: chloroform, toluene, benzene, and carbon disulfide in ultraviolet, visible, and near-infrared, J. Appl. Phys. 94 (2003) 6167–6174.
[36] H. Fukuda, M. Oda, Copolymerization of ketene cyclic N,O-acetals with carbon disulfide: evidence for formation of Zwitterionic Intermediates by means of ^1H NMR spectroscopy, Macromolecules 29 (1996) 3043–3045.
[37] G.H. Signhal, R.L. Espino, J.E. Sobel, G.A. Huff, Hydrodesulfurization of sulfur heterocyclic compounds, J. Catal. 67 (1981) 457–458.
[38] V.R. Choudhary, A.K. Kinage, T.V. Choudhary, Low-temperature nonoxidative activation of methane over H-galloaluminosilicate (MFI) Zeolite, Science 275 (1997) 1286–1288.
[39] T.H. Maugh 2nd, Methane C-H bonds activated, Science 222 (1983) 315.
[40] P. He, J. Jarvis, L. Liu, H. Song, The promoting effect of Pt on the co-aromatization of pentane with methane and propane over Zn-Pt/HZSM-5, Fuel 239 (2019) 946–954.
[41] P. He, J.S. Jarvis, S. Meng, Q. Li, G.M. Bernard, L. Liu, X. Mao, Z. Jiang, H. Zeng, V. K. Michaelis, H. Song, Co-aromatization of methane with propane over Zn/HZSM-5: The methane reaction pathway and the effect of Zn distribution, Appl. Catal. B: Environ. 250 (2019) 99–111.
[42] S. Sharifvaghefi, B. Yang, Y. Zheng, New insights on the role of H_2S and sulfur vacancies on dibenzothiophene hydrodesulfurization over MoS_2 edges, Appl. Catal. A: Gen. 566 (2018) 164–173.
[43] P. He, J. Jarvis, S. Meng, A. Wang, S. Kou, R. Gatip, M. Yung, L. Liu, H. Song, Co-aromatization of methane with olefins: The role of inner pore and external surface catalytic sites, Appl. Catal. B: Environ. 234 (2018) 234–246.
[44] Z. Paál, T. Koltai, et al., , Sulfur uptake and exchange, HDS activity and structure of sulfided, Al_2O_3 supported MoO_x, $PdMoO_x$ and $PtMoO_x$ catalysts, Phys. Chem. Chem. Phys. 3 (2001) 1535–1543.
[45] V.L. Sushkevich, A.G. Popov, I.I. Ivanova, Sulfur-33 Isotope tracing of the hydrodesulfurization process: insights into the reaction mechanism, catalyst characterization and improvement, Angew. Chem. 56 (2017) 10872–10876.
[46] P. Gao, X. Chen, M. Hao, F. Xiao, S. Yang, Oxygen vacancy enhancing the Fe_2O_3-CeO_2 catalysts in Fenton-like reaction for the sulfamerazine degradation under O_2 atmosphere, Chemosphere 228 (2019) 521–527.
[47] B. Shen, X. Chen, D. Cai, H. Xiong, X. Liu, C. Meng, Y. Han, F. Wei, Atomic spatial and temporal imaging of local structures and light elements inside zeolite frameworks, Adv. Mater. 32 (2020), e1906103.
[48] B. Shen, X. Chen, H. Wang, H. Xiong, E.G.T. Bosch, I. Lazic, D. Cai, W. Qian, S. Jin, X. Liu, Y. Han, F. Wei, A single-molecule van der Waals compass, Nature 592 (2021) 541–544.
[49] Y. Lou, P. He, L. Zhao, W. Cheng, H. Song, Olefin Upgrading over Ir/ZSM-5 catalysts under methane environment, Appl. Catal. B: Environ. 201 (2017) 278–289.
[50] K. Nakamura, A. Okuda, K. Ohta, H. Matsubara, K. Okumura, K. Yamamoto, R. Itagaki, S. Suganuma, E. Tsuji, N. Katada, Direct methylation of benzene with methane catalyzed by Co/MFI Zeolite, ChemCatChem 10 (2018) 3806–3812.
[51] Z. Shen, P. He, A. Wang, J. Harrhy, S. Meng, H. Peng, H. Song, Conversion of naphthalene as model compound of polyaromatics to mono-aromatic hydrocarbons under the mixed hydrogen and methane atmosphere, Fuel 243 (2019) 469–477.
[52] X. Zhang, V. Ponce, D.E. Galvez-Aranda, G. Zhou, H. Zhou, J.M. Seminario, CS_2 removal from C5 distillates by reactive molecular dynamics simulations, Ind. Eng. Chem. Res. 60 (2021) 5816–5825.